THE UNIVERSITY OF MICHIGAN

COLLEGE OF ENGINEERING
Department of Mechanical Engineering
Heat Transfer and Thermodynamics Laboratory

Final Report
(including material for Quarterly Progress Report No. 3
for the period July through September 1960)

PRESSURIZATION OF LIQUID OXYGEN CONTAINERS

J. A. Clark
H. Merte, Jr.
V. S. Arpaci
M. Starr
P. Fennema
J. Beukema
S. Eshghy
H. Law

ORA Project 03583

under contract with:

DEPARTMENT OF THE ARMY
DETROIT ORDNANCE DISTRICT
CONTRACT NO. DA-20-018-506-ORD-254
DETROIT, MICHIGAN

administered through:

OFFICE OF RESEARCH ADMINISTRATION ANN ARBOR

March 1961

TABLE OF CONTENTS

ABSTRACT

This constitutes the final report on the subject contract. Material included herein is that which also describes the results of research effort during the third quarter, July to October, 1960. Owing to an increased rate of expenditure during the summer of 1960, funds for this research were expended by October, 1960. This increased rate of expenditure resulted from the addition of research personnel during the summer whose services became available then and who could and did contribute materially to the program. The increased rate of expenditure had the prior approval of the sponsoring agency. Owing to these circumstances, no fourth quarterly progress report will be issued on this contract.

An orderly progress of research has been maintained, however, by the continuation of this work under the sponsorship of the NASA through the George C. Marshall Space Flight Center at Huntsville, Alabama, starting October 1, 1960.

The following major topics are reported on herein:

I. Optimization of pressurized-discharge processes in cryogenic containers.

II. Boiling of a cryogenic fluid under reduced gravity.

III. Heat transfer to a cryogenic fluid in an accelerating system.

I. OPTIMIZATION OF PRESSURIZED-DISCHARGE PROCESSES IN CRYOGENIC CONTAINERS

A. EXPERIMENTAL PROGRAM

During the past quarter, the new system has been put into operation. Figure 1 represents schematically the flow diagram of the system and its component parts. The principal change from the previous system is the incorporation of an annular container around the main container, which is discussed later. Figures 2, 3, and 4 are photographs showing the general view of the experimental setup and its filling apparatus. The main control consul, Sanborn and Minneapolis-Honeywell oscillographic recorders, thermocouple switches, and nitrogen pressurization bottles are shown in Fig. 2. A view of the electrical heater controls for both the main container and the annular container as well as the insulated container assembly is shown in Fig. 3. Figure 4 is a photograph showing the insulated container assembly connected by means of an insulated transfer line and quick opening valves to a large, portable liquid nitrogen storage vessel.

The pressurized-discharge container consists of two components, a cylindrical container (Fig. 5) and an annular container (Fig. 6). A sectional view of the two containers and the interior construction is shown in Fig. 7. Both containers are fabricated of 1/8-in. 5052 aluminum except for the end plates which are 1/2-in. aluminum. The cylindrical container has a diameter of 1.02 ft and the annular container has diameters of 1.25 and 1.67 ft. Both are 3 ft in length. The containers are connected hydrau-

lically at top and bottom by the inlet and discharge lines so that filling, pressurizing, and discharging is accomplished simultaneously in both containers and with equal liquid levels in each. The inside top of the main, or cylindrical, container is insulated with a 1-in.-thick layer of styrofoam to reduce the heat-transfer interaction between the top and the pressurizing gas, and therefore reduce an "end effect" in the system. The outside of the annular container is wrapped with approximately two inches of Fiberglas to reduce heat-transfer interaction with the ambient. This may be seen in Figs. 3 and 4.

The principal function of the annular container is to provide an automatically adjusting and matching thermal guard for the main container. This enables a reasonably accurate measurement of heat flux to be imposed on the main container. Chromel A heater ribbon is attached with Scotch thermo-setting tape to the outside of the main container and to the inside of the annular container, as is noted in Figs. 5 and 6. These are designed so that an identical heat flux is imposed on each container for the heat flux runs. Subsequent experience with this type of heating indicated an inadequacy except at low heat flux. At high heat flux (2000 Btu/hr-ft^2 in this study) the heater ribbon appeared to expand and pull away from the main container, thus introducing an uncertainity in the imposed wall heat flux. This will be discussed in greater detail in later reports of this laboratory, and alternate methods of heating will be proposed. The heater circuit wiring diagram is shown in Fig. 8. For heat exchange with the ambient, it is necessary to remove the annular container from the assembly.

A total of 25 thermocouples is arranged at various locations throughout the system as shown in Fig. 9. One thermocouple is used to measure the pressurizing gas temperature at the exit from the diffuser at the top of the tank, the point of which the gas enters the main container. Eight thermocouples are imbedded into the main container wall to measure its temperature. At four axial positions directly opposite four of the main container wall thermocouples, the temperature of the inside annular wall is measured. These measurements are taken to determine the effectiveness of the annular container in eliminating the temperature difference between its wall and that of the main container. At selected radial and axial locations in the main container, eight additional thermocouples, fixed in position, measure the temperature of the gas space. Since these are fixed position thermocouples, they are immersed in the liquid nitrogen until the liquid-gas interface passes. Because of their inherent heat capacity and the fact that gas condenses on them as they break the liquid surface, they do not measure the gas temperature reliably in the region of the interface. The measurement of temperatures in this region has been accomplished by four thermocouples which move with the interface and are always exposed to the gas. These thermocouples are mounted on the float of the level indicator and extend above the liquid-gas interface into the gas phase. This arrangement is shown in Fig. 10 and may also be seen in Fig. 7. In this way, a reliable monitoring of the gas temperature near the interface is obtained.

Two different recording instruments are used in these studies. A 36-channel Minneapolis-Honeywell oscillograph model 1012 "Visicorder" records

the temperatures of the walls of both containers and the temperature of the gas space in the main container. A 4-channel Sanborn (150 series) oscillograph records the weight of the liquid in the containers by means of a load cell, the level of the liquid nitrogen in the main container, the main container pressure by means of a pressure transducer, and the temperature of the pressurizing gas at the inlet to the main container. A typical Sanborn record for a run is shown in Fig. 11.

The level indicator consists of what is essentially a potentiometer circuit with a moving contact attached to a float. A general view of the indicator is shown in Fig. 10. The float consists of two segments of an annular ring of HD2 styrofoam. Slide wipers are mounted on a framework which is attached to this float. The wiper arrangement is made of two directly opposed copper slides mounted on arms which are hinged about a common axis at the surface of the float. This arrangement maintains the wipers directly opposed at all times, even when the float pitches and rolls as it does when the liquid boils violently. Initially, one of the wires was made of chromel and the other copper, but excessive corrosion and subsequent unreliable contact between the slide and the wire made necessary a replacement of the copper wire with another of similar diameter but made of chromel. Figure 12 is the wiring diagram. Prior to filling the main container with liquid nitrogen, it was found necessary to purge the container with dry nitrogen gas. This eliminated water vapor from the tank space which would condense on the level-indicator voltage wires, insulating them from the wipers and reducing the effectiveness of the level-measuring system.

The purpose of the level indicator has been three-fold. It is used to determine the velocity of the interface, as illustrated in Fig. 11, since it enables the determination of float location as a function of time. It can be used to determine the position of the liquid-gas interface, and thus the position of the floating thermocouples relative to the interface at any time throughout the run. Measurements indicate that the uncertainty of this indicator in determining liquid level is 1/16 in. The level indicator also has been used to determine bubble hold-up volume in the container, by measuring the drop in the level of the indicator upon the pressurization of the boiling liquid in the container. The bubble hold-up volume is then the product of the level drop and the cross-sectional area of the container. Figure 13 is a Sanborn oscillographic record showing the change in level of the float during pressurization and de-pressurization. From these data the total bubble volume in the liquid prior to pressurization can be found. It can also be noted from Fig. 13 that upon de-pressurization a greater vapor volume is formed that was initially present. This appears to result from flashing of the liquid which was heated somewhat during the time the liquid was pressurized as the vapor volume returned to essentially its original value following de-pressurization.

Bottled dry nitrogen gas was used as the pressurizing gas for all the experimental runs reported. To obtain the quantity of flow necessary to maintain a constant pressure during discharge, a surge tank is incorporated into the system (Fig. 1). Before starting discharge, the surge tank is pressurized to a high (100 psig) pressure, so that, when discharge begins, the

pressure rises in the main container very quickly to 35 psig. A regulator automatically maintains a constant discharge pressure of 35 psig throughout the run, as can be seen in Fig. 11. Two heat exchangers are utilized to obtain various values of inlet gas temperature. For the inlet gas temperatures between 0 and 100°F a boiling-water heat exchanger is used, and for the low temperatures, a liquid nitrogen heat exchanger is used. A variation in inlet gas temperature between the values +100°F and -300°F is obtained by selectively wetting the surface of the heat exchangers with liquid nitrogen or boiling water and then allowing the ambient to heat or cool the pressurant to the desired inlet temperature.

B. EXPERIMENTAL DATA

The general purpose of the experimental system is to determine the variation of the mean density of the residual gas in the tank with a number of parameters which are imposed on the system. The gas space temperatures at the end of the run, as obtained from the various thermocouples in the system, are plotted versus distance in the tank for each run. This plot is then integrated with a planimeter and the (spatial) mean temperature is computed. From this and the pressure, the (spatial) mean gas density is obtained using an equation of state.

The main parameters which are varied as the independent variables in the system are inlet gas temperatures and container wall heat flux. The inlet gas temperature is controlled over a range of from -300°F to +100°F by use of two heat exchangers as described above. Heat flux conditions have been adiabatic, heat exchange with the ambient, and imposed heat flux of

1000 Btu/hr-ft^2 and 2000 Btu/hr-ft^2. Higher heat fluxes are expected to be used in the future. Another parameter which can be varied is the type of pressurant used. Nitrogen gas has been used primarily up to now, but it is expected that helium gas will be employed in the future. Time of discharge has been held constant at approximately 120 sec but may also be varied in future runs. Likewise, the discharge pressure has also been fixed at 50 psia in these runs. Future plans include changing the parameter to other levels.

The following table catalogues all the experimental runs since August, 1959, listing the magnitude of the various parameters. For the runs from 44 to 49, not all the heat flux data were used for correlation. This resulted from uncertainty in the values of the heat flux imposed because, owing to expansion on heating, the heater wires altered their position on the tank wall. For these runs correlation was poor. This was the primary reason for re-wiring the tank, using heater ribbon having special mounting to prevent loss of alignment. Even this method does not appear to give results which are up to standard in reliability, as indicated above.

SUMMARY OF EXPERIMENTAL DATA SINCE AUGUST, 1959

Run No.	Date	T_g	P	θ	q"	m_i	n	Remarks
44A	8/25/59	+ 36	48.4	76.5	Adb	87.5	1	Pressure fluctuated: disregarded
44B	8/25/59	+ 43	39.4	58.4	Adb	70.0	1	Pressure fluctuated: disregarded
44C	8/26/59	+ 40	49.4	105.6	Adb	95.0	1	Data used for correlation
44D								No data collected
44E	8/27/59	- 3	48.8	104.0	1255	103.0	1	Data not used for correlation
44F	8/27/59	- 12	48.3	91.1	Adb	102.0	1	Data used for correlation
44G	8/27/59	- 2	49.3	107.2	1270	104.0	1	Data not used for correlation
44H	8/27/59	- 12	49.3	117.0	Adb	105.0	1	Data used for correlation
44I	8/27/59	- 4	49.3	125.2	1275	107.0	1	Data not used for correlation
44J	8/28/59	+ 40	49.2	99.2	Adb	106.0	1	Data used for correlation
44K								No data collected
44L								No data collected
44M	9/14/59	+ 7	48.8	100.4	1225	98.0	1	Data not used for correlation
44N	9/14/59	- 2	48.35	101.0	1250	99.0	1	Data not used for correlation
45A	9/2/59	+ 76	44.17	102.1	Adb	105.0	1	Pressure too low: disregarded
45B	9/2/59	+ 79	49.17	106.4	1260	100.0	1	Data not used for correlation
45C	9/2/59	+ 63	45.17	108.4	Adb	102.0	1	Pressure too low: disregarded
45D	9/3/59	+ 90	48.56	115.6	Adb	102.0	1	Data used for correlation
45E	9/3/59	+103	48.56	130.3	1240	107.0	1	Data not used for correlation
45F	9/3/59	+ 98	49.36	110.3	Adb	97.5	1	Data used for correlation
45G	9/3/59	+103	48.46	119.3	1260	101.0	1	Data not used for correlation
45H	9/3/59	+ 98	47.36	111.0	Adb	106.0	1	Pressure too low: disregarded
45I	9/14/59	+ 81	49.35	122.1	1225	97.0	1	Data not used for correlation
45J	9/14/59	+ 77	49.35	104.1	1225	91.0	1	Data not used for correlation
46A	9/3/59	-299	47.36	98.8	Adb	97.5	1	Pressure too low: disregarded
46B	9/3/59	-125	48.36	100.7	Adb	98.0	1	Data used for correlation
46C	9/3/59	-269	50.36	97.4	1200	102.5	1	T_g fluctuated: disregarded
46D	9/3/59	- 32	46.36	99.7	1234	105.0	1	Pressure too low: disregarded
46E	9/3/59	- 77	47.36	90.3	1254	95.0	1	Pressure too low: disregarded
46F	9/3/59	- 50	47.36	79.2	Adb	87.0	1	Pressure too low: disregarded
46G	9/14/59	- 26	49.35	111.1	Adb	108.0	1	Data used for correlation
46H	9/14/59	-256	44.36	125	Adb	107.5	1	Pressure too low: disregarded
46I	9/14/59	-103	48.85	108.4	Adb	110.0	1	Data used for correlation
46J	9/14/59	- 66	48.35	111.2	Adb	112.0	1	Data used for correlation
46K	9/14/59	-226	44.35	100	Adb	110.0	1	Data used for correlation
47A	10/22/59	-183	49.34	107.4	Adb	103.0	1	Data used for correlation
47B	10/22/59	-206	47.34	101	Adb	103.5	1	Pressure too low: disregarded
47C								No data collected
47D	10/22/59	-228	49.34	106.6	1209	107.5	1	Data not used for correlation
47E								No data collected
47F	10/29/59	-213	49.46	109.5	Adb	107	1	Data used for correlation
47G	10/29/59	-244	48.46	109.9	Adb	111	1	Data used for correlation
47H	10/29/59	-173	48.96	107.3	Adb	112	1	Data used for correlation
47I	10/29/59	-159	48.46	107.6	Adb	110	1	Data used for correlation
47J	10/29/59	-123	40.46	120.8	1186	111	1	Pressure too low: disregarded
47K	10/29/59	-204	49.46	107.1	1200	106	1	Data not used for correlation
47L	10/29/59	-274	49.46	111.1	1216	107	1	Data not used for correlation
47M	10/29/59	-225	48.96	116.0	1209	112	1	Data not used for correlation
48A	11/12/59	+ 22	48.4	118.2	3240	110	1	Data not used for correlation
48B	11/12/59	+ 15	53.4	108.7	2100	108	1	Pressure too high: disregarded
48C	11/12/59	-244	48.4	119.0	2240	108	1	Data not used for correlation
48D	11/12/59	-248	49.4	122.9	2248	112	1	Data not used for correlation
48E	11/12/59	+ 94	53.4	102.7	2220	106	1	Pressure too high: disregarded
48F	11/12/59	+ 59	54.4	109.0	2324	108	1	Pressure too high: disregarded
48G	11/12/59	+ 81	34.4	147.0	2228	97	1	Pressure too low: disregarded
49A	11/12/59	+ 22	52.9	98.3	3306	97	1	Pressure too high: disregarded
49B	11/12/59	+ 12	52.4	114.3	3090	110	1	Data not used for correlation
49C	11/12/59	-212	47.4	116.9	3114	100	1	Pressure too low: disregarded
49D	11/12/59	-270	48.9	134.6	3134	113	1	Heaters off before discharge
49E	11/12/59	-266	54.9	107.2	2843	110	1	Pressure too high: disregarded
49F	11/12/59	+ 94	54.9	118.5	3006	107	1	Pressure too low: disregarded
49G	11/12/59	+ 94	54.9	109.4	3030	99	1	Pressure too high: disregarded
49H	12/23/59	-220	51.50	103.7	2871	95	1	Data not used for correlation
49I	12/29/59	-270	49.06	111.8	2695	105	1	Data not used for correlation
49J	12/29/59	-252	44.06	142.8	2651	104	1	Pressure too low: disregarded
49K	12/29/59	-102	49.06	164.5	2687	109	1	Data not used for correlation

SUMMARY OF EXPERIMENTAL DATA SINCE AUGUST, 1959 (Concluded)

Run No.	Date	T_g	P	θ	q"	m_i	n	Remarks
49L	12/29/59	-102	49.06	119.9	2690	98	1	Data not used for correlation
49M	12/29/59	+ 74	49.06	125.3	2691	103	1	Data not used for correlation
49N	12/29/59	+ 94	49.06	106.2	2719	90	1	Data not used for correlation
490	12/29/59	+ 94	48.06	133.2	2727	100	1	Data not used for correlation
49P	12/29/59	+ 98	99.06	166	2747	100	1	Data not used for correlation
50A	12/21/59							Exploratory long discharge time run; no data collected
50B	1/29/60							Exploratory long discharge time run; no data collected
51A	7/26/60	+ 54	52.7	89.5	Amb	100	2	Data used for correlation
51B	7/27/60	+ 94	46.7	98	Amb	78	2	Pressure too low: disregarded
51C	7/27/60	+ 94	47.7	107	Amb	90	2	Data used for correlation
51D	7/27/60	+ 36	47.7	114.5	Amb	91	2	Data used for correlation
51E	7/27/60	+ 22	46.7	113	Amb	95	2	Data used for correlation
51F	7/27/60	+ 52	42.7	112	Amb	104	2	Data used for correlation
52A	8/9/60	+ 77	41.4	127.5	Adb	190	2A	Data used for correlation
52B	8/9/60	+ 98	44.4	109	Adb	182	2A	Data used for correlation
52C	8/15/60	+ 95	46.41	114	Adb	193	2A	Data used for correlation
52D	8/15/60	-120	52.41	119	Adb	209	2A	Data used for correlation
52E	8/16/60	+ 74	49.41	117	Adb	203	2A	Data used for correlation
52F	8/16/60	-102	50.41	121	Adb	203	2A	Data used for correlation
52G	8/16/60	- 71	49.41	113	Adb	206	2A	Data used for correlation
52H	8/16/60	- 48	49.41	117	Adb	202	2A	Data used for correlation
52I	8/17/60	+ 8	49.41	117	Adb	203	2A	Data used for correlation
52J	9/1/60	-138	50.4	103	Adb	210	2A	Data used for correlation
52K	9/1/60	-228	46.4	124	Adb	220	2A	Data used for correlation
52L	9/7/60	-186	50.3	123	Adb	220	2A	Data used for correlation
52M								No data collected
52N	9/7/60	- 96	50.3	111	Adb	212	2A	Data used for correlation
520	9/7/60	-168	49.3	123	Adb	220	2A	Data used for correlation
52P	9/7/60	- 11	49.3	120	Adb	222	2A	Pressure fluctuated: disregarded
52Q	9/7/60	+ 31	49.3	122	Adb	230	2A	Pressure fluctuated: disregarded
53A	8/10/60	+ 82	49.41	118	542	198	2A	Data used for correlation
53B	8/9/60	+ 88	49.41	116	1083	185	2A	Data used for correlation
53C	8/15/60	+ 95	47.41	119	1083	203	2A	Data used for correlation
53D	8/15/60	-144	53.41	107	1083	193	2A	Pressure too high: disregarded
53E	8/16/60	+ 86	49.41	119	1083	205	2A	Data used for correlation
53F	8/16/60	- 98	50.41	113	1083	202	2A	Data used for correlation
53G	8/16/60	- 52	49.41	115	1083	202	2A	Data used for correlation
53H	8/16/60	- 48	49.41	120	1083	204	2A	Data used for correlation
53I	8/17/60	+ 4	48.41	117	1083	203	2A	Data used for correlation
53J	9/1/60	-197	50.4	106	1083	219	2A	Data used for correlation
53K	9/7/60	-132	49.3	124	1083	232	2A	Data used for correlation
53L	9/7/60	-186	50.3	118	1083	221	2A	Data used for correlation
53M	9/7/60	-154	50.3	119	1083	219	2A	Data used for correlation
53N	9/7/60	-158	50.3	121	1083	218	2A	Data used for correlation
530	9/7/60	+ 17	50.3	119	1083	222	2A	Data used for correlation
54A	8/15/60	+ 98	52.4	124	2166	204	2A	Data used for correlation
54B	8/15/60	-156	52.41	111	2166	186	2A	Data used for correlation
54C	8/16/60	+ 91	50.41	122	2166	206	2A	Data used for correlation
54D	8/16/60	- 88	50.41	122	2166	199	2A	Data used for correlation
54E	8/16/60	- 50	49.41	117	2166	204	2A	Data used for correlation
54F	8/16/60	- 77	49.41	121	2166	204	2A	Data used for correlation
54G	8/17/60	+ 2	49.41	122	2166	289	2A	Data used for correlation
54H	9/1/60	-190	49.9	110	2166	212	2A	Data used for correlation
54I	9/7/60	-160	50.3	128	2166	218	2A	Data used for correlation
54J	9/7/60	-183	50.3	124	2166	219	2A	Data used for correlation
54K	9/7/60	-176	50.3	124	2166	219	2A	Data used for correlation
54L	9/7/60	-183	49.3	126	2166	220	2A	Data used for correlation
54M	9/7/60	+ 26	50.3	122	2166	220	2A	Data used for correlation
54N	9/7/60	+ 31	49.3	122	2166	230	2A	Data used for correlation

T_g = Inlet gas temperature, °F
P = Discharging pressure, psia
θ = Discharge time, second
q" = Heat flux, Btu/hr-ft^2
m_i = Initial weight, lbm
n = Tank model number

Tank Model Designations

a. Tank number 1 refers to the tank as sketched in Fig. 2 of UMRI Report 2646-16-P, May, 1959.

b. Tank number 2 refers to the same tank as (a) above, except that heater ribbon is used in place of heater wire, and Scotch thermo-setting tape instead of asbestos. The tape is interwoven with the ribbon to help hold the ribbon in place.

c. Tank number 2A refers to the same tank as (a) and (b) but with the annular guard tank mounted. Tank model assembly 2A is shown in Fig. 7.

C. ANALYSIS OF GAS- AND WALL-TEMPERATURE RESPONSE DURING THE DISCHARGE OF A CRYOGENIC LIQUID FROM A CONTAINER

The following analysis has been described and presented in Quarterly Progress Report No. 2, August, 1960, but owing to its bearing on experimental results obtained since and also to the character of this report, it is included here.

The basic physical system analyzed is shown in Fig. 14. This consists of a cylindrical container from which the cryogenic liquid is discharged by means of a pressurizing gas.

The first case considers the container exchanging heat with the ambient through a convection heat-transfer coefficient. The second case considers an arbitrary heat flux imposed on the outer surface of the container. The proper combination of the separate parts of the analysis, which is discussed below, provides the solution for simultaneous heat transfer with the ambient

and an imposed heat flux. This combination closely approximates the conditions imposed on cryogenic containers on space vehicles where both heat transfer with the ambient and external heat flux may be expected to occur.

The following assumptions are made: (a) the velocity transient at the start of discharge of the liquid from the container is small compared to the thermal transients and therefore is neglected; (b) the axial conduction of heat is neglected in both the container wall and in the pressurizing gas; (c) the radial temperature distribution in both the container wall and the pressurizing gas are ignored, the temperature in each being lumped; (d) average convection heat-transfer coefficients are assumed to be constant; (e) physical properties of both container wall and pressurizing gas are constant; and (f) the dynamic response of the system is introduced by two sources: (i) change in the temperature of the pressurizing gas at the inlet of the container and/or (ii) the imposition of a heat-transfer interaction with the ambient. The heat-transfer interaction with the ambient consists of two separate modes: (a) heat transfer through a convection coefficient of heat transfer with an ambient at constant temperature and (b) an imposed heat flux on the outer wall of the container.

It has been observed from experimental measurements that the liquid and wall temperatures below the liquid-gas interface had a negligibly small variation during the period of the discharge of the liquid from the container. This results from the fact that the liquid is at a saturated state corresponding to the initial pressure, and acts as a heat sink at constant temperature. Furthermore, it has a very large heat capacity and has a low

thermal resistance between it and the wall. Therefore, in the following analysis, heat transfer between the container and the ambient is assumed negligible for all regions below the liquid-gas interface. This is accomplished by assuming, in Case I, a constant ambient temperature equal to the liquid temperature below the liquid-gas interface, and in Case II, an imposed constant heat flux above the liquid-gas interface only. Thus, in Case I, the ambient moves with the liquid-gas interface, wetting only that part of the container wall above the interface, and in Case II, the imposed heat flux moves with the liquid-gas interface, affecting only that part of the container wall above the interface.

In both these cases the difficulty arising from assuming the same convection coefficients of heat transfer above and below the liquid-gas interface is eliminated as had been previously done and reported.

The differential equations from the First Law of Thermodynamics with associated initial-boundary conditions for this system are:

For the gas:

$$\frac{\partial T}{\partial \theta} + V \frac{\partial T}{\partial x} + b_1(T - t) = 0 \tag{1}$$

For the container wall:

$$\frac{\partial t}{\partial \theta} - b_2(T-t) - \begin{Bmatrix} b_3(T_a-t) \\ \phi \end{Bmatrix} = 0 \tag{2}$$

$$T(x,o) = T_\ell \tag{3}$$

$$t(x,o) = T_\ell \tag{4}$$

$$T(o,\theta) = T_g \tag{5}$$

where T_ℓ is the saturated liquid temperature and T_g is the temperature of the pressurizing gas at the inlet to the container. In Eq. (2), $b_3(T_a-t)$ corresponds to Case I, the moving ambient, where

$$T_a = \begin{cases} T_a \ , \ x \leqslant V\theta \\ T_\ell \ , \ x > V\theta \end{cases} \tag{6}$$

and ϕ corresponds to Case II, the moving heat flux, where

$$\phi = \begin{cases} \phi \ , \ x \leqslant V\theta \\ o \ , \ x > V\theta \end{cases} \tag{7}$$

The method of analysis for both cases is essentially the same and therefore only Case I will be carried out in detail. The results of Case II will be presented.

1. Method of Analysis

a. Case I - Moving Ambient.—Upon scaling all temperatures to the saturation temperature of the liquid, the energy equations for Case I become:

$$\frac{\partial T^*}{\partial \theta} + V \frac{\partial T^*}{\partial x} + b_1(T^* - t^*) = 0 \tag{8}$$

$$\frac{\partial t^*}{\partial \theta} - b_2(T^* - t^*) + b_3(t^* - T_a^*) = 0 \tag{9}$$

$$T^*(x,o) = 0 = T(x,o) - T_\ell \tag{10}$$

$$t^*(x,o) = 0 = t(x,o) - T_\ell \tag{11}$$

$$T^*(o,\theta) = T_g^* \tag{12}$$

$$T_a^* = \begin{cases} T_a^* , & x \leqslant V\theta \\ o , & x > V\theta \end{cases} \tag{13}$$

For mathematical convenience only, the above problem can be separated into the following two problems in which $T^* = T_1+T_2$ and $t^* = t_1+t_2$, as follows,

$$\frac{\partial T_1}{\partial \theta} + V \frac{\partial T_1}{\partial x} + b_1(T_1 - t_1) = 0 \tag{14}$$

$$\frac{\partial t_1}{\partial \theta} - b_2(T_1 - t_1) + b_3(t_1 - o) = 0 \tag{15}$$

$$T_1(x,o) = 0 \tag{16}$$

$$t_1(x,o) = 0 \tag{17}$$

$$T_1(o,\theta) = T_g^* \tag{18}$$

$$\frac{\partial T_2}{\partial \theta} + V \frac{\partial T_2}{\partial x} + b_1(T_2 - t_2) = 0 \tag{19}$$

$$\frac{\partial t_2}{\partial \theta} - b_2(T_2 - t_2) + b_3(t_2 - T_a^*) = 0 \tag{20}$$

$$T_2(x,o) = 0 \tag{21}$$

$$t_2(x,o) = 0 \tag{22}$$

$$T_2(o,\theta) = 0 \tag{23}$$

The solution of Eqs. (14)-(18) is obtained by the use of the Laplace Transformation in the timewise domain. The subsidary equation in terms of

the gas temperature, T_1, is,

$$\frac{d\bar{T}_1}{dx} + \frac{1}{V}\left(p + b_1 - \frac{b_1 b_2}{p+b}\right)\bar{T}_1 = 0 \tag{24}$$

with the transformed boundary condition,

$$\bar{T}_1(o,p) = T_g^*/p \tag{25}$$

where

$$b = b_3 + b_2 \tag{26}$$

The solution of the above equation is obtained directly from the methods of treating ordinary differential equations. It is

$$\frac{\bar{T}_1}{T_g} = \frac{1}{p} e^{-\frac{x}{V}p} \cdot e^{-\frac{b_1 x}{V}} \cdot e^{\frac{b_1 b_2 x}{V(p+b)}} \tag{27}$$

Combining Eq. (27) with the Laplace transformation of Eq. (15), the transformed wall temperature is found to be:

$$\frac{\bar{t}_1}{T_g^*} = b_2 e^{-\frac{x}{V}p} \cdot e^{-\frac{b_1 x}{V}} \cdot \frac{e^{\frac{b_1 b_2 x}{V(p+b)}}}{p(p+b)} \tag{28}$$

The inverse transforms of Eqs. (27) and (28) can be obtained by the use of a table of Laplace Transforms;[1] they are:

$$\frac{T_1}{T_g^*} = e^{-s}\left\{\psi(\eta s, \frac{\delta}{\eta}) + e^{-\frac{\delta}{\eta}} I_o[2(s\delta)^{1/2}]\right\}, \quad x \leqslant V\theta \tag{29}$$

$$\frac{t_1}{T_g^*} = \eta\, e^{-s}\, \psi(\eta s, \frac{\delta}{\eta}), \qquad x \leqslant V\theta \tag{30}$$

where

$$\psi(\eta s, \frac{\delta}{\eta}) \equiv \int_0^{\delta/\eta} e^{-\frac{\delta^*}{\eta}}\, I_0[2(s\delta^*)^{1/2}]\, \frac{d\delta^*}{\eta} \tag{31}$$

$$s \equiv \frac{b_1 x}{V} \tag{32}$$

$$\delta \equiv b_2(\theta - \frac{x}{V}) \tag{33}$$

$$\eta \equiv \frac{b_2}{b_2+b_3} \tag{34}$$

I_0 designates the modified Bessel function of the first kind zero order. The function ψ, defined by Eq. (31), has been obtained and calculated previously by Rizika,[2] where it is presented in graphical form.

The solution of Eqs. (19)-(23), which is the main concern of this analysis, is also obtained by the Laplace Transformation method. In this case it is convenient to use the Laplace transform in both the time and the space domains.

Taking the Laplace transformation of Eqs. (19)-(23) in the x (space) domain results in the following two transformed equations with the appropriate initial conditions:

$$\frac{d\bar{T}_2}{d\theta} + Vq\bar{T}_2 + b_1(\bar{T}_2 - \bar{t}_2) = 0 \tag{35}$$

$$\frac{d\bar{t}_2}{d\theta} - b_2(\bar{T}_2 - \bar{t}_2) + b_3\bar{t}_2 - b_3\frac{T_a^*}{q}\left(1-e^{-V\theta q}\right) = 0 \tag{36}$$

$$\bar{T}_2(q,o) = 0 \tag{37}$$

$$\bar{t}_2(q,o) = 0 \tag{38}$$

Defining

$$\Delta(x,\theta) = t_2 - T_2 \tag{39}$$

the container wall-gas temperature difference, the transformed container wall and gas temperatures can be found in terms of $\bar{\Delta}$ where $\bar{\Delta}$ is the Laplace transformed (in the x variable) temperature difference. They are:

$$\bar{T}_2 = b_1 \int_o^\theta e^{-Vq(\theta-\theta^*)} \bar{\Delta}(q,\theta^*)d\theta^* \tag{40}$$

$$\bar{t}_2 = \frac{T_a^*}{q}\left(1-e^{-b_3\theta}\right) + \frac{b_3 T_a^*}{q(b_3-Vq)}\left(e^{-b_3\theta} - e^{-Vq\theta}\right) - b_2 \int_o^\theta e^{-b_3(\theta-\theta^*)} \bar{\Delta}(q,\theta^*)d\theta^* \tag{41}$$

Taking the double Laplace transform of Eq. (39) with respect to x and θ, and the Laplace transform of Eqs. (40)-(41) with respect to θ, and combining produces,

$$\bar{\bar{\Delta}} = \frac{T_a^* b_3}{p(p+b)\left[\frac{p}{V} + \frac{b_1}{V}\left(\frac{p+b_3}{p+b}\right) + q\right]} \tag{42}$$

The inverse transformation of the foregoing equation with respect to x is

$$\bar{\Delta}(x,p) = \frac{T_a^* b_3}{p(p+b)} e^{-\left[\frac{p}{V} + \frac{b_1}{V}\left(\frac{p+b_3}{p+b}\right)\right] x} \tag{43}$$

On the other hand, the timewise Laplace transformation of the energy equation for the gas Eq. (19), in terms of $\bar{\Delta}$ can be written as follows:

$$p\bar{T}_2 + V\frac{d}{dx}\bar{T}_2 - b_1\bar{\Delta} = 0 \tag{44}$$

$$\bar{T}_2(o,p) = 0 \tag{45}$$

Combining Eqs. (43) and (44) and solving for $\bar{T}_2(x,p)$, and subjecting the solution to the boundary condition, Eq. (45), produces:

$$\bar{T}_2(x,p) = \frac{T_a^* b_3}{p(p+b_3)} e^{-\frac{p}{V}x} - \frac{T_a^* b_3}{p(p+b_3)} \frac{e^{-\frac{b_1}{V}\left(\frac{p+b_3}{p+b}\right)x}}{p+b} e^{-\frac{p}{V}x} \tag{46}$$

Using the timewise transform in Eqs. (39) and (46) results in the transformed temperature of the container wall, as follows:

$$\frac{\bar{t}_2(x,p)}{T_a^*} = \frac{b_3}{p(p+b_3)} e^{-\frac{p}{V}x} - \frac{b_2 b_3}{p(p+b_3)} e^{-\frac{p}{V}x} \cdot e^{-\frac{b_1 x}{V}} \cdot \frac{e^{\frac{b_1 b_2 x}{V(p+b)}}}{(p+b)} \tag{47}$$

Using Laplace transform tables,[1] the inverse of Eqs. (46)-(47) are

$$\frac{T_2(x,\theta)}{T_a^*} = 1 - e^{-s}\,\psi\left(\eta s, \frac{\delta}{\eta}\right) - e^{\left(\delta - \frac{\delta}{\eta}\right)}\left[1 - e^{-s}\,\psi(s,\delta)\right], \quad x \leqslant V\theta \tag{48}$$

$$\frac{t_2(x,\theta)}{T_a^*} = (1-\eta) + \eta\left[1 - e^{-s}\,\psi\left(\eta s, \frac{\delta}{\eta}\right)\right] - e^{\left(\delta - \frac{\delta}{\eta}\right)}\left[1 - e^{-s}\,\psi(s,\delta)\right], \quad x \leqslant V\theta \tag{49}$$

where ψ, which is defined previously, occurs with two different parameter systems (s,δ) and $\left(\eta s, \frac{\delta}{\eta}\right)$.

The solution of the problem as stated at the beginning is the linear combination of T_1 and T_2, Eqs. (29) and (48), and t_1 and t_2, Eqs. (30) and (49).

b. Case II - Moving Heat Flux.—For the case of the moving heat flux, Eqs. (1)-(5) can be conveniently separated into the following two problems when the temperature is scaled to the saturation temperature of the liquid:

$$\frac{\partial T_1}{\partial \theta} + V \frac{\partial T_1}{\partial x} + b_1(T_1 - t_1) = 0 \tag{50}$$

$$\frac{\partial t_1}{\partial \theta} - b_2(T_1 - t_1) = 0 \tag{51}$$

$$T_1(x,o) = 0 \tag{52}$$

$$t_1(x,o) = 0 \tag{53}$$

$$T_1(o,\theta) = T_g^* \tag{54}$$

and

$$\frac{\partial T_2}{\partial \theta} + V \frac{\partial T_2}{\partial x} + b_1(T_2 - t_2) = 0 \tag{55}$$

$$\frac{\partial t_2}{\partial \theta} - b_2(T_2 - t_2) - \phi = 0 \tag{56}$$

$$T_2(x,o) = 0 \tag{57}$$

$$t_2(x,o) = 0 \tag{58}$$

$$T_2(o,\theta) = 0 \tag{59}$$

where ϕ is defined in Eq. (7). Actually the solution of Eqs. (50)-(54) for T_1 and t_1 is a special case of the solution of Eqs. (14)-(18) where $b_3 = 0$ and hence $\eta = 1$. This special case has been solved.[2]

The second part, Eqs. (55)-(59) for T_2 and t_2, is solved in a manner similar to that used for solving Eqs. (19)-(23). The results are

$$\frac{T_2(x,\theta)}{\phi/b_2} = \delta + e^{-s}\left[\Lambda(s,\delta) - (1+\delta)\psi(s,\delta)\right], \quad x \leqslant V\theta \tag{60}$$

$$\frac{t_2(x,\theta)}{\phi/b_2} = \delta + e^{-s}\left[\Lambda(s,\delta) - \delta\psi(s,\delta)\right], \quad x \leqslant V\theta \tag{61}$$

where δ, s, and ψ have been defined previously and

$$\Lambda(s,\delta) \equiv \int_0^{\delta} \delta^* e^{-\delta^*} I_o\left[2(s\delta^*)^{1/2}\right] d\delta^* \tag{62}$$

The function $\Lambda(s,\delta)$ has been calculated and is presented in graphical form.[3]

The linear combination of Eqs. (29) and (30) with $\eta = 1$ and Eqs. (60) and (61) will yield the solution of the dynamic response of the gas and wall temperature of a pressurized container having an imposed wall heat flux.

The combination of the solutions for the moving ambient case, Eqs. (29) and (48) and Eqs. (30) and (49), Case I, and the solutions of the second part of the moving heat flux case, Eq. (60) and Eq. (61), Case II, will provide the solution for the case in which both heat transfer with the ambient and an imposed heat flux occur.

2. Summary of Theoretical Results

For convenience in using these results, they are presented in the following dimensionless form in which the various combinations indicated above have been performed.

a. Case I - Moving Ambient.—

(i) Pressurizing gas, $x \leqslant V\theta$

$$\frac{T(x,\theta)-T_\ell}{T_g-T_\ell} = e^{-s}\left\{\psi(\eta s,\frac{\delta}{\eta}) + e^{-\frac{\delta}{\eta}} I_o\left[2(s\delta)^{1/2}\right]\right\} + \frac{T_a-T_\ell}{T_g-T_\ell}\left\{1-e^{-s}\psi(\eta s,\frac{\delta}{\eta}) - e^{-\frac{\delta}{\eta}(1-\eta)}\left[1-e^{-s}\psi(s,\delta)\right]\right\} \tag{63}$$

(ii) Container wall, $x \leqslant V\theta$

$$\frac{t(x,\theta)-T_\ell}{T_g-T_\ell} = \frac{T_a-T_\ell}{T_g-T_\ell}\left\{(1-\eta) + \eta\left[1-e^{-s}\psi(\eta s,\frac{\delta}{\eta})\right] - e^{-\frac{\delta}{\eta}(1-\eta)}\left[1-e^{-s}\psi(s,\delta)\right]\right\} + \eta e^{-s}\psi(\eta s,\frac{\delta}{\eta}) \tag{64}$$

b. Case II - Moving Heat Flux.—

(i) Pressurizing gas, $x \leqslant V\theta$

$$\frac{T(x,\theta)-T_\ell}{T_g-T_\ell} = e^{-s}\left\{\psi(s,\delta) + e^{-\delta} I_o\left[2(s\delta)^{1/2}\right]\right\} + \frac{q''P_o/\bar{h}_g P}{T_g-T_\ell}\left\{\delta + e^{-s}\left[\Lambda(s,\delta)-(1+\delta)\psi(s,\delta)\right]\right\} \tag{65}$$

(ii) Container wall, $x \leqslant V\theta$

$$\frac{t(x,\theta)-T_\ell}{T_g-T_\ell} = \frac{q''P_o/\bar{h}_g P}{T_g-T_\ell}\left\{\delta + e^{-s}\left[\Lambda(s,\delta) - \delta\psi(s,\delta)\right]\right\} + e^{-s}\psi(s,\delta) \tag{66}$$

Two functions $\psi(\eta s,\frac{\delta}{\eta})$ or $\psi(s,\delta)$ and $\Lambda(s,\delta)$ have been given in a previous progress report[4] and are necessary for the calculations of $T(x,\theta)$ and $t(x,\theta)$ using Eqs. (63)-(66). The function $\psi(\eta s,\frac{\delta}{\eta})$ or $\psi(s,\delta)$ is presented here in Fig. 15. This function has been found and is tabulated by Rizika.[2] The function $\Lambda(s,\delta)$ has been found and is tabulated.[3] This function is presented here in Fig. 16. At the moment both function ψ and Λ have been programmed on the IBM 704 for a numerical tabulation which makes their use more convenient and practical than the curves given.

In Eqs. (63)-(66) the quantities s, δ and η are defined as:

$$s = \frac{\bar{h}_g P}{\rho C_p A} \frac{x}{V} \tag{67}$$

$$\delta = \frac{\bar{h}_g P}{\rho' C_p' A_o} \left(\theta - \frac{x}{V}\right) \tag{68}$$

$$\eta = \frac{1}{1 + \bar{h}_o P_o / \bar{h}_g P} \tag{69}$$

3. Influence of System Parameters on Gas Temperature Response

Equations (63)-(66) describe the response of both the wall and gas temperatures for the boundary conditions of an imposed ambient temperature (moving ambient) and an imposed heat flux (moving heat flux). In this section the influence of the system parameters on the response of the gas temperature for the case of a transient introduced by heat transfer with the ambient (moving ambient) is examined. Similar analyses can be done for the case of the moving heat flux and also including the influence of the system parameters on the wall temperature, but for the sake of brevity the analysis for the gas temperature alone will be presented. Sufficient detail will be given, however, so that the other cases could be carried out if desired.

For the case of the moving ambient, the response of the gas temperature is given by Eq. (63), which may be written as

$$\begin{aligned} \frac{T(x,\theta)-T_\ell}{T_g-T_\ell} &= \frac{T_1(x,\theta)}{T_g-T_\ell} + \frac{T_2(x,\theta)}{T_g-T_\ell} \\ &= \frac{T_1(x,\theta)}{T_g-T_\ell} + \frac{T_a-T_\ell}{T_g-T_\ell} \cdot \frac{T_2(x,\theta)}{T_a-T_\ell} \end{aligned} \tag{70}$$

in which

$$\frac{T_1(x,\theta)}{T_g-T_\ell} = e^{-s}\left\{\psi(\eta s,\frac{\delta}{\eta}) + e^{-\frac{\delta}{\eta}} I_o\left[2(s\delta)^{1/2}\right]\right\} \tag{71}$$

and

$$\frac{T_2(x,\theta)}{T_g-T_\ell} = \left(\frac{T_a-T_\ell}{T_g-T_\ell}\right)\left\{1 - e^{-s}\psi(\eta s,\frac{\delta}{\eta}) - e^{-\frac{\delta}{\eta}(1-\eta)}\left[1-e^{-s}\psi(s,\delta)\right]\right\} \tag{72}$$

Thus, it may be seen that the dimensionless gas temperature response may be written:

$$\frac{T(x,\theta)-T_\ell}{T_g-T_\ell} = f\left[s,\delta,\eta,\frac{T_a-T_\ell}{T_g-T_\ell}\right] \tag{73}$$

The term $(T_a-T_\ell)/(T_g-T_\ell)$ may be imposed on the system arbitrarily and indicates the manner by which the influence of the ambient is introduced into the theoretical results. The parameters s, δ and η are defined above in Eqs. (67), (68), and (69) in terms of the system parameters and time. The parameter s is made up of properties of the gas and $\frac{x}{V}$ and may be considered a gas parameter; the parameter δ is made up of wall properties, θ and $\frac{x}{V}$, and may be considered a wall parameter. The parameter η introduces the effect of the relative convective heat transfer between the gas-and-wall and wall-and-ambient. A value of η = 0.5 indicates approximately equal convective coefficients $\bar{h}_o$ and $\bar{h}_g$, whereas a value of η greater than 0.50 corresponds to conditions for which $\bar{h}_g$ is greater than $\bar{h}_o$. The range of possible values for η is from 0 to 1.0, with the more probable range for these experiments being from 0.50 to 1.0, i.e., for $\bar{h}_g$ greater than $\bar{h}_o$.

To show the influence of s, δ, and η on the gas temperature, two plots have been prepared for two values of η. Figure 17 is for $\eta = 0.75$ and Fig. 18 is for $\eta = 0.50$. Each plot gives $T_1(x,\theta)/(T_g-T_\ell)$ and $T_2(x,\theta)/(T_a-T_\ell)$ as a function of s with δ as the parameter. The dimensionless gas temperature $(T(x,\theta)-T_\ell)/(T_g-T_\ell)$ is formed from Eq. (70) and thus requires the specification of the ratio $(T_a-T_\ell)/(T_g-T_\ell)$ in addition to the functions $T_1(x,\theta)/(T_g-T_\ell)$ and $T_2(x,\theta)/(T_a-T_\ell)$ of Figs. 17 and 18 to complete its calculation. However, for a value of $\frac{T_a-T_\ell}{T_g-T_\ell}$ equal to 1.0, Figs. 17 and 18 may be employed directly to obtain $\frac{T(x,\theta)-T_\ell}{T_g-T_\ell}$, which will be discussed later.

The absolute value of the gas temperature is written from Eq. (70) as

$$T(x,\theta) = T_\ell + (T_g-T_\ell)\left[\frac{T_1(x,\theta)}{T_g-T_\ell}\right] + (T_a-T_\ell)\left[\frac{T_2(x,\theta)}{T_a-T_\ell}\right] \tag{74}$$

Hence, large values of $T(x,\theta)$ and low gas density may be expected to correspond to large values of (T_g-T_ℓ), high inlet temperatures, and large values of (T_a-T_ℓ), high ambient temperatures. In pressurized discharge systems for cryogenic liquids T_ℓ is usually fixed by the choice of liquid. Actually, it will be observed from Eq. (70), and also on physical grounds, that a high gas temperature and lower gas density results from the ratio $(T_a-T_\ell)/(T_g-T_\ell)$ being larger than 1.0, as this corresponds to T_a being greater than T_g, and heat is thus transferred to the wall and then to the pressurizing gas at least in the upper portions of the container.

Large values of $T(x,\theta)$ also are associated with large values of the ratios $T_1(x,\theta)/(T_g-T_\ell)$ and $T_2(x,\theta)/(T_a-T_\ell)$. These two important ratios are

given in Figs. 17 and 18 for η equal to 0.75 and 0.50, respectively. The parameter is δ, the wall parameter and the abcissa is s, the gas parameter. For the conditions for which these curves are drawn $T_1(x,\theta)/(T_g-T_\ell)$ is the significant quantity governing for the range of s from 0 to about 2 and 3, and for s greater than this quantity $T_2(x,\theta)/(T_a-T_\ell)$ appears to be the significant quantity.

What becomes evident from these results is that a high value of gas temperature (low gas density) is to be expected with low values of s, high values of δ and low values of η. Thus, this may be summarized by observing that for high values of $T(x,\theta)$, the following conditions should be obtained.

a. Low Value of s: Since $s = \frac{\bar{h}_g P}{\ell C_p A V} \cdot x$, this condition corresponds to a small value of gas space heat transfer coefficient, $\bar{h}_g$, and perimeter to flow area ratio, $\frac{P}{A}$. A small value of $\frac{P}{A}$ is obtained with containers having a circular cross section of large diameter. In addition, a low value of s is obtained with high discharge rates (large interface velocity V) and employing a gas as a pressurant having a large heat capacity C_p and density ρ, although the latter is somewhat contradictory for those conditions for minimum mean gas density in the container. As is discussed later, it is desirable to select a pressurant and the conditions of pressurization conducive to small gas density. In regards to C_p, a large value of this is desired to achieve small values of s. It is important to note relative to this requirement the exceptionally large values of C_p for hydrogen and helium gas. At room temperature C_p for hydrogen is approximately 16 times that of oxygen, and helium about 6 times greater than oxygen.

b. High Value of δ: since $\delta \equiv \frac{\bar{h}_g P}{\rho' C_p' A_o} (\theta - \frac{x}{V})$, this quantity is made large by large $\bar{h}_g$ and $\frac{P}{A_o}$. An increase in $\bar{h}_g$ is contrary to that corresponding to small s and thus it is difficult to generalize on this quantity. The importance of the magnitude of this parameter will probably depend on the conditions of the discharge process and it seems better to decide each case separately. However, in a great many instances it probably will be desirable to have $\bar{h}_g$ as small as possible, if this is a controllable variable. A large $\frac{P}{A_o}$ ratio is obtained by using container walls having small thickness. For large δ it is further desirable that the wall be of a material having a low product of $\rho' C_p'$. The condition on the use of these results is that $\theta \geqslant \frac{x}{V}$ but within this a large interface velocity V will contribute to an increased δ.

c. Low Value of η.—Low values of η correspond to large values of the ratio $\bar{h}_o P_o / \bar{h}_g P$. This condition is associated most practically with $\bar{h}_o$ being greater than $\bar{h}_g$. Under these circumstances the heat transfer to the container from the ambient becomes very significant and is reflected in the results of $T(x,\theta)$.

To indicate these influences directly, the dimensionless gas temperature $(T(x,\theta)-T_\ell)/(T_g-T_\ell)$ is plotted in Fig. 19 against s for values of η = 0.50, and 0.75 and δ = 0.25 and 1.0 and for the ratio $\frac{T_a-T_\ell}{T_g-T_\ell} = 1$, i.e., for $T_a = T_g$. A similar set of curves for other values of $(T_a-T_\ell)/(T_g-T_\ell)$ may be constructed from Figs. 17 and 18 for η = 0.50 and 0.75.

Minimum pressurizing gas density is a function of other variables as well. For most low pressure gases the density is written

$$\rho = \frac{P}{RT} = \frac{PM}{\bar{R}T}$$

Hence, the density is also minimized for conditions corresponding to lowest possible level of pressure and the use of a gas with small molecular weight. In this respect attention is drawn once again to helium and hydrogen as desirable pressurants.

4. Calculation Procedure

The gas and wall temperature distributions over the length of the container are found from the equations derived from the theoretical analysis. In the analysis, $\bar{h}_g$, the inside heat-transfer coefficient, $\bar{h}_o$, the outside heat-transfer coefficient, $\rho'C_p'$, the heat capacity of the wall, and ρC_p, the heat capacity of the gas, are treated as invariants. Since constancy of $\rho'C_p'$ is a fair approximation an average value of $\rho'C_p'$ for aluminum (6061-T6) at -260°F is used in all the calculations.

Owing to the uncertainity in estimating the values of $\bar{h}_o$ and $\bar{h}_g$, several values (in this case from 1 through 4 Btu/hr-ft^2-°F) are chosen and the results of these calculations are compared with the experimental data. The values of $\bar{h}_g$ and $\bar{h}_o$ used in the theory which most closely correspond to the experimental data are taken to be those which may be used to describe the heat transfer. In the experimental model, $\bar{h}_o$ = 1 and $\bar{h}_g$ = 2 Btu/hr-ft^2-°F appear to give the best results in the moving ambient case. Also $\bar{h}_g = 2 \frac{\text{Btu}}{\text{hr-ft}^2\text{-°F}}$ seems to be a proper value for moving heat flux case. These results are discussed later in this report.

5. Determination of Mean Gas Density for use in the Theoretical Equations

Obtaining the correct value for ρ, the mean gas density is accompanied by a trial and error process. First a mean temperature $T_m = \frac{1}{2}(T_\ell + T_g)$ is assumed. This provides a mean density to be used in gas temperature equations. Then the gas temperature distribution is calculated and a new mean temperature is obtained. The next step is to plot the computed mean temperature against the assumed mean temperature. Each trial will provide a point on such a plot. Another mean temperature is assumed and calculations are repeated. A straight line through two such points normally will suffice to define the locus of assumed vs. calculated mean temperatures. The intersection of this line and a 45° line passing through the origin will determine the true mean temperature. The true mean density then will be obtained using the equation of state.

Figure 20 shows a number of points obtained for this process on a computed temperature-assumed temperature plot. For each inlet gas temperature, there are two points through which a straight line is drawn. The points on Fig. 20 are the calculation results for an adiabatic container having $\bar{h}_g$ = 2 Btu/hr-ft^2-°F.

This trial and error process must be repeated for every inlet gas temperature to obtain the mean density as a function of the inlet gas temperature from the theory. Thus, for each inlet gas temperature, the true mean density is known. Using values of the mean density so determined, it is possible to calculate the wall temperature distribution without having to repeat any of the trial and error process.

D. COMPARISON OF THEORY WITH EXPERIMENT

The use of these analytical results requires a knowledge of the system parameters. One of the most important of these but also one about which little is known is $\bar{h}_g$, the average gas-space heat-transfer coefficient. Owing to the relative uncertainity surrounding an a priori determination of $\bar{h}_g$, these theoretical results are computed for a range of values of $\bar{h}_g$ of from 1 to 4 $\frac{\text{Btu}}{\text{hr-ft}^2\text{-}^\circ\text{F}}$ and then compared with experimental data, the purpose being to establish an approximate magnitude for this quantity which will adequately represent the system. Figure 21 is a plot of mean density vs. inlet gas temperature for the above-mentioned range. This figure has been computed for an adiabatic container. The comparison with experimental data shows that the analytical curve for $\bar{h}_g = 2 \frac{\text{Btu}}{\text{hr-ft}^2\text{-}^\circ\text{F}}$ closely approximates the data. The rest of the calculations have been carried out for $\bar{h}_g = 2$ and 3 Btu/hr-ft^2-°F. It is important to note in regard to these results that a calculation of $\bar{h}_g$ from established heat-transfer correlations for free convection[5] corresponding to the conditions of the experiments (Figure 21) give a value between 2 and 3 Btu/hr-ft^2-°F. Since this also is the range of values for which the theory and the experiments are in agreement, these results suggest that the convective heat-transfer processes within the gas space are governed largely by free convection. Whatever influence may be introduced by the axial flow resulting from discharge apparently is not large, at least for these experiments where the interfacial velocity was approximately 0.025 ft/sec. As an estimate (yet unchecked), it might be anticipated that these processes will remain to be controlled by free convection as long

as the Grashof number is very much greater than the Reynolds number based on discharge velocity. The effect of increased discharge velocity will probably tend to increase the value of $\bar{h}_g$. The comparison of theory with experiment is separately discussed for the two basic cases, namely, the moving ambient case and the moving heat flux case.

1. Moving Ambient Case

In this case there is heat exchange between the ambient and the tank wall through a heat-transfer coefficient $\bar{h}_o$. The corresponding gas-temperature response is given by Eq. (63). Assuming that $\bar{h}_g$ is essentially the same as in the adiabatic container, an approximate value of $\bar{h}_o$ can be determined by comparing experimental data with analytical results calculated for $\bar{h}_g = 2 \frac{\text{Btu}}{\text{hr-ft}^2\text{-°F}}$ and for several values of $\bar{h}_o$. Figure 22 indicates that $\bar{h}_o = 1$ Btu/hr-ft^2-°F is a reasonable value for the average outside coefficient of heat transfer.

Figure 23 is a plot of gas-temperature distribution 90 seconds after beginning of discharge. As may be seen in this plot, theory and experiment agree very closely for $\bar{h}_g = 2$. Note that in the region of the interface, the floating thermocouples indicate a sharp temperature gradient, whereas at this point the theory predicts a sudden change from gas temperature to the initial liquid saturation temperature. The fixed thermocouple 3 inches above the liquid-gas interface measures slightly below the theoretical temperature at that point. This probably results from the thermal lag of the thermocouple owing to its heat capacity and its relatively recent emergence from the liquid bulk.

Figure 24 shows the wall-temperature distribution as computed with the theory, Eq. (64), for three inlet gas temperatures. Experimental results for an inlet gas temperature of 482R are shown. It will be observed that the experimental data fall above but are closely parallel to the theoretical curve. It is believed that this results primarily from the use of T_ℓ = 140°R in Eq. (64), the same value of T_ℓ as for the gas-temperature response, Eq. (63). Whereas T_ℓ = 140°R is reasonable for the gas temperature, it has been observed in experiment that owing to heat transfer with the ambient and to condensation of pressurizing gas on the cold wall in the region of the interface, the wall actually enters the gas space at a somewhat higher temperature. Should this be allowed for in the theory, it would cause the curves in Fig. 24 to fall higher and move in line with the experimental results. As an indication of this, the saturation temperature at 50 psia, the pressure of gas, is shown on Fig. 24, which could be used as a base for the theoretical curves.

2. Moving Heat Flux Case

In this case the heat transfer is imposed in the form of a constant heat flux on the outer surface of the container. The theoretical model for this case has the heat flux imposed only on that portion of the wall above the liquid-gas interface and, thus, must move down the wall with the speed of the interface. Hence the name "moving heat flux," as described above. The response of both gas and wall temperatures is given by Eqs. (65) and (66), respectively.

As a special case of the moving heat flux an adiabatic, or zero heat flux condition (q" = 0), will first be studied. This is convenient as it is

possible to control an adiabatic condition experimentally quite practically, thus providing a check of the theory for this limiting condition. It will be observed that Eqs. (65) and (66) for this condition (q" = 0) become identical with the corresponding results for the moving ambient case, Eqs. (63) and (64) when $\eta = 1$ (i.e., $\bar{h}_o = 0$), as would be necessary.

Experimental results for comparison with the theory, Eqs. (65) and (66), for q" = 0 are given in Figs. 25-27. These data were taken with the apparatus shown in Figs. 2-7. The annular container acted as the thermal guard providing an accurately controllable adiabatic environment for the container. As may be observed, a fairly favorable comparison is obtained between the theory for both the gas and wall temperatures for this case.

Comparison of the theoretical results with experimental data for the case of finite heat flux is given in Figs. 28-33. The range of heat flux (q") in these data is from 0 to 2166 Btu/hr-ft^2. The experimental apparatus employed is that shown in Figs. 2-7. The heating effect is obtained from the disipation of electric current in electrical resistance ribbon tightly wound around the test container in four separately controlled sections, as described previously. Electrical power is measured by a Weston 310 wattmeter, and the heat flux is found from the ratio of measured electrical power to the outside container area covered by the resistance wire.

At the lower heat flux (up to 1083 Btu/hr-ft^2), the agreement between theory and data is reasonably favorable. These results are given in Figs. 28-30. However, a tendency for the experimental data to fall below the theoretical curve is observed. This is especially true of the wall temperature

at the upper sections of the container. The gas temperatures as measured by both the floating and fixed thermocouples are in notable agreement, as seen in Fig. 29. In general, however, up to approximately 1083 Btu/hr-ft^2 heat flux, the theory and experimental data are in reasonable accord.

At higher heat flux a distinct departure is observed between the theory and experimental data. This comparison is found in Figs. 31 and 32, which show the gas- and wall-temperature distributions corresponding to a heat flux of 2166 Btu/hr-ft^2. The departure is most strikingly evident in Fig. 32 where the wall temperature is measured at the container top to be as much as 200°F below the theoretical prediction.

An examination of the wall temperatures in the annular guard disclosed the probably reason for this discrepancy. The annular guard wall temperatures were much higher than those in the container wall at corresponding elevations in the upper regions of the assembly. This suggested the possible expansion of the heater ribbon away from the container at the higher heat flux, thus reducing significantly the transfer or heat to the container itself with, consequently, a much lower measured wall temperature in those regions. (This was later confirmed to be the case and will reported later.) An opposite effect would, of course, be found on the annular tank since expansion of the heater ribbon would tend to cause the wire to be pressed more closely to the wall.

From these results it appears necessary to abandon the use of externally wound electrical resistance wire for heat flux measurements, at least in the higher ranges of heat flux. At the moment consideration is being given

to the design of a radiant device for the transfer of a specified heat flux.

It is felt that the departure of theory and data at these higher heat fluxes is not a result of an inadequate theory, but that the present experimental system did not impose the same conditions on the physical system as used in the theory.

A summary of the data for the moving heat flux case is given in Fig. 33 which shows the final mean gas density as a function of inlet gas temperature for a range of heat flux. The solid lines represent the theory. As may be seen, the gas densities fall away from the theory at the higher heat flux. The theory probably predicts a truer result and the difference may be attributed to those effects discussed above.

II. BOILING OF A CRYOGENIC FLUID UNDER REDUCED GRAVITY

The test platform as described in Quarterly Progress Report No. 2, 1960, has been constructed, and is shown in Fig. 34. A 74-lb dummy load is mounted on the platform to simulate the test package during preliminary drop tests to check the performance of the buffer assembly in decelerating the test platform.

The buffer assembly was received from the manufacturer during this period. After several tests, it was apparent that the test platform was receiving too large an initial shock upon impact with the buffer piston, due to the necessity of accelerating the piston before the declerating action of the hydraulic oil can become effective. To reduce this shock, the mass of the piston was reduced to approximately half its original value by reducing the wall thickness. In addition, a heavy-duty spring was mounted on the piston. As the spring is compressed, it serves to accelerate the piston before contact with the test platform is made, reducing the impact.

Figure 35 is a view of the hydraulic buffer assembly and shows the test platform as it would appear at the moment of impact.

To obtain a quantitative measure of the impact shock and of the performance of the buffer assembly, a 1000-g piezoelectric accelerometer is mounted on the test platform and a strain-gage-type pressure transducer is mounted on the buffer piston face. The accelerometer measures the deceleration of the test platform and the pressure transducer records the pressure behavior in the hydraulic cylinder. The data will be displayed simultaneously on a

dual-beam oscilloscope and recorded with a polaroid camera. This information will permit the evaluation of the techniques to be attempted in reducing the initial impact shock.

A test-platform release mechanism has been constructed and tested, with satisfactory performance. The platform is suspended by a single 17-gage chrome "A" wire. To release the platform, the wire is melted by passing through it approximately 50 amp from a 220-v source by means of clips spaced 1/2 in. apart. Figure 36 is a view of the burning wire mechanism, showing the wire, clips, and the electrical contact which swings free as the platform drops.

The release mechanism has two major advantages over a mechanical type. No side forces are imposed on the test platform during release and the physical parting of the wire link permits the determination of the instant of release by electrical measurements.

Safety interlocks are provided so that the test platform cannot be released unless certain necessary conditions are fulfilled. These conditions are indicated by lights on the control panel and are as follows:

1. The buffer piston must be in its uppermost position.
2. The door of the safety enclosure surrounding the buffer must be closed.
3. The "basement ready" switch must be closed by the observer at the basement level.
4. The "platform ready" switch must be closed at the upper platform level.

When these conditions are fulfilled, the platform may be released from the control panel by closing a "drop" switch.

The safety interlock system is diagrammed in Fig. 37.

A three-station intercom system has been installed to permit voice communication between the control panel, basement level, and upper platform level.

The 0- to 1-g accelerometer to be used in measuring the platform accelerating during its drop has been received from the manufacturer. It is rated to withstand a maximum acceleration of 50 g's. Should the impact upon deceleration be greater than this, the accelerometer will be shock-mounted to protect it.

Attempts are presently being made to reduce the initial impact and will be continued during the next period. An insulated container for the liquid nitrogen test package is being constructed. A 1/2-in. aluminum sphere has been obtained for use as a calorimeter in the transient boiling process and is being instrumented. Preliminary tests will be made at normal gravity before installation of the reduced gravity test platform.

III. HEAT TRANSFER TO A CRYOGENIC FLUID IN AN ACCELERATING SYSTEM

The construction of the hardware for the test vessel to be used with a cryogenic fluid has been completed. The test vessel was shown in Fig. 18 of Quarterly Progress Report No. 2, 1960. Assembly is approximately 75% complete, requiring only calibration of the thermocouples to continue.

The thermocouples, used for measuring heater surface and liquid temperatures, are being calibrated at three fixed points; the mercury freezing point, equilibrium between solid and vapor CO_2, and equilibrium between liquid and vapor nitrogen.

Three thermocouples, 1/32-in. OD, are inserted radially in the heater cylinder at the same level, 1/16 in. below the heater surface to obtain an average temperature. The surface temperature will be calculated by extrapolating the measured temperature to the surface, using a temperature gradient calculated from the measured heat flux.

With the present apparatus it is not possible to condense the vapor nitrogen due to boiling, nor continuously to replenish the supply of liquid nitrogen with the system under rotation. To keep the time required for the heater surface temperature to attain the possible new steady-state value due to acceleration as short as possible, the thermal inertia of the heater block must be as low as possible. Hence, the heater block is made as thin as possible consistent with a thickness sufficient to smooth irregularities in heat flux which may be present at the face in contact with the electrical heater resistance elements.

Figure 38 shows a cross section of the heater assembly. The heating suface is one end of a copper disc 3 in. in diameter by 3/4 in. thick. A thin copper skirt, 0.002 in. thick, is soldered around the edge to provide a continuous surface and at the same time keep the heat losses by conduction from the periphery to a minimum. Woods metal (meltin point = 87°C) was used as the solder metal to avoid deformation of the thin copper skirt which would otherwise occur with the normal type of soft solders. The thickness of the copper disc does not permit inserting thermocouples at different levels to measure the temperature gradient. With this configuration the heat flux is expected to be below 25,000 Btu/hr-ft^2, and the error due to extrapolating the measured temperature using a calculated temperature gradient is expected to be small.

The construction of the mercury slip ring, described in Quarterly Progress Report No. 2, 1960, for transmitting a stable, large d-c current to the rotating number has been completed and tested. Upon applying 6 v d-c to a resistive load such that a current of 8 amp was drawn through the slip ring, the variation in current upon rotation was 1.5 ma peak-to-peak at twice the rotational frequency. By doubling the voltage for the same current, the variation was reduced to less than 1 ma peak-to-peak, as might be expected. The variation occurs because it was necessary to split the pairs of slip ring rods in semi-circular segments for assembly purposes. Every half revolution the orientation of the rings is such that the electrical resistance path through the mercury is increased by a slight amount. This could be eliminated by a major design change, but is not deemed desirable at this stage.

Upon assembly of the test vessel described above and completion of experimental runs for boiling data from the flat plate, the mercury slip ring will be used to obtain data on the influence of acceleration (increased force fields) upon the peak heat flux with a cryogenic fluid. In the interim, some preliminary data will be obtained with water as the boiling fluid to determine if the trends are consistent with fluids of widely varying properties.

Figure 39 shows a preliminary design of a cylindrical heater configuration wherein the acceleration vector will be parallel to the heating surface. Such a configuration will permit the investigation of the influence of heating surface orientation on the boiling characteristics of a cryogenic fluid in the presence of force fields greater than normal gravity.

Tubular heater elements are to be tightly coiled and inserted within a copper ring. The spaces between will be filled with a metal such as soft solder to conduct the heat from the heater elements to the copper ring. The outer surface of the copper ring acts as the heat-transfer surface. By the judicious use of insulating materials and air spaces, the heat losses through the ends of the cylinder will be kept at a minimum, providing the desired radial flow of heat through the copper ring. Thermocouples in the copper ring will be used for measuring the surface temperature.

It is anticipated that with this orientation, the contribution of non-boiling convective heat transfer with increasing acceleration will be quite significant. To isolate the contribution due to boiling, the sequence of the experimental program will be first to employ the flat plate heater, where the

acceleration vector is normal to the heated surface, and then to conduct the experiments with the cylindrical heating surface, where the acceleration vector is parallel to the heating surface.

REFERENCES

1. Campbell, G. A., and Foster, R. M., Fourier Integrals, Van Nostrand Co., 1948, p. 79, Par. 655.1.

2. Rizika, J. W., Trans. ASME, No. 78, 1407 (1956).

3. Arpaci, V. S., and Clark, J. A., Trans. ASME, 80, p. 625-634 (1958).

4. Clark, J. A., Arpaci, V. S., et al., No. 2, UMRI 03583, University of Michigan, Ann Arbor, Michigan, July, 1960.

5. McAdams, W. H., Heat Transmission, third edition, McGraw-Hill, 1954.

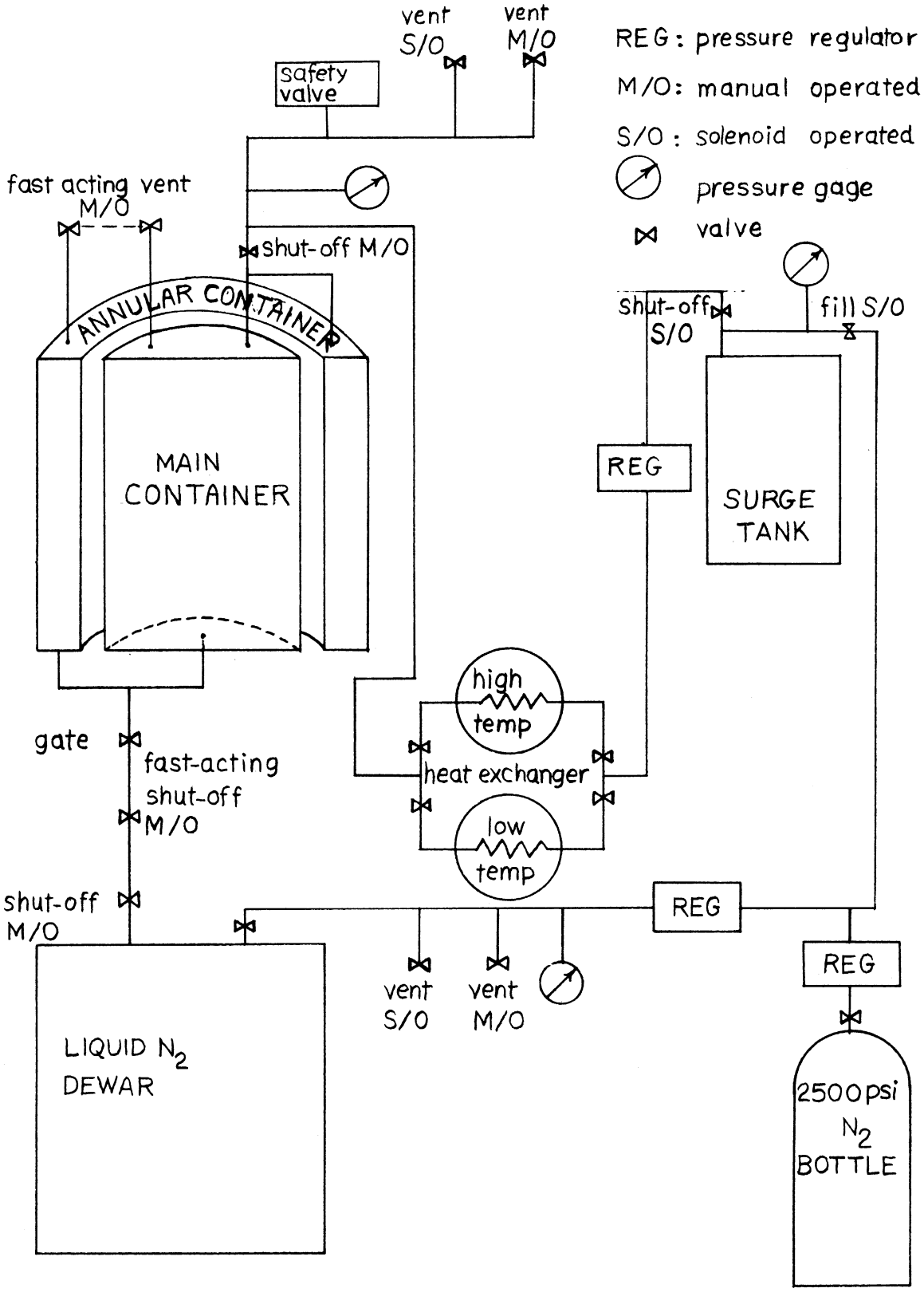

Fig. 1. System for pressurized discharge test.

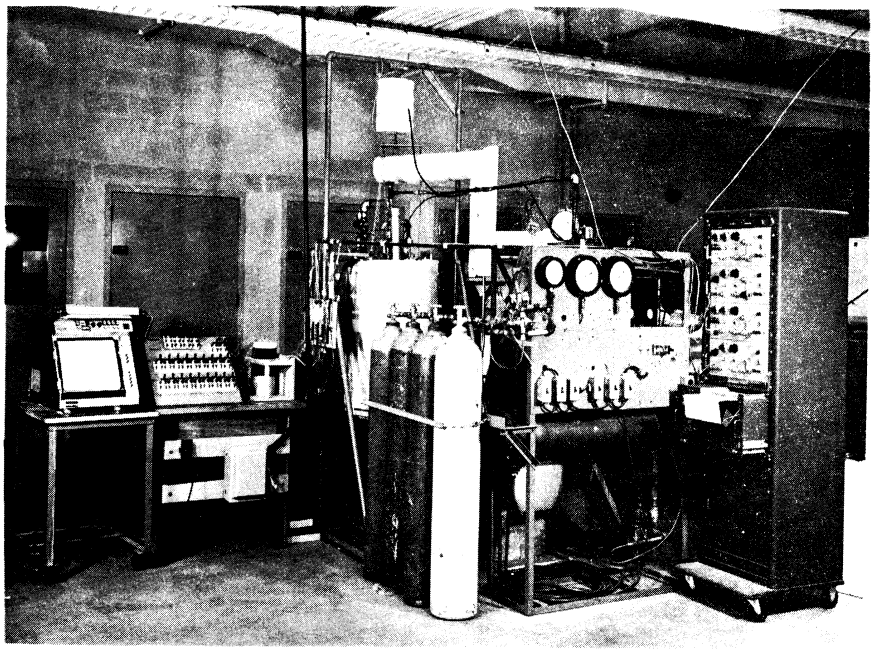

Fig. 2. Photograph of experimental apparatus.

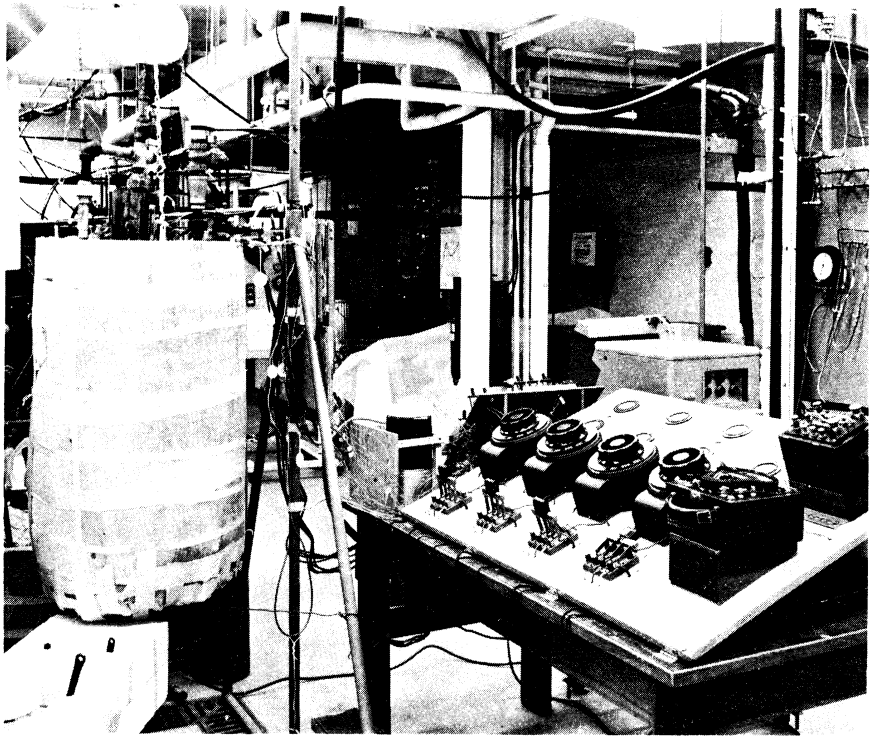

Fig. 3. Photograph of experimental apparatus.

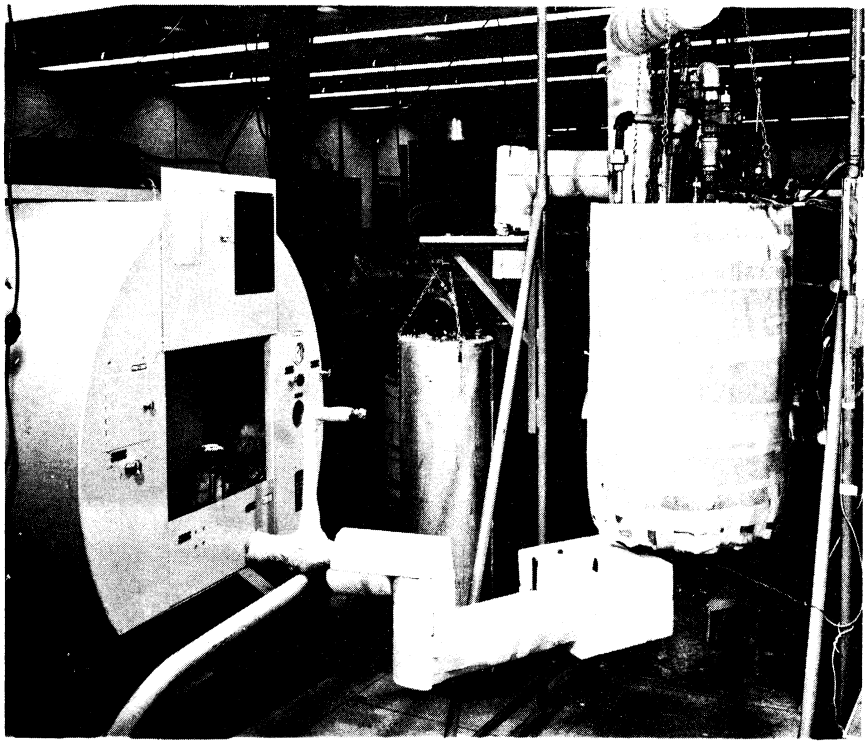

Fig. 4. Photograph showing liquid nitrogen filling apparatus.

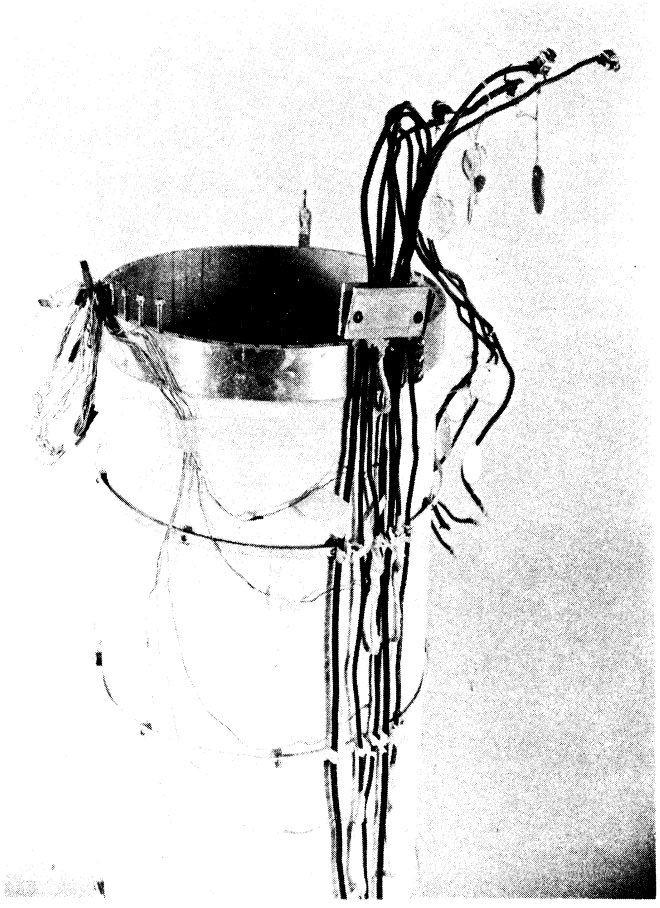

Fig. 5. Photograph of main container.

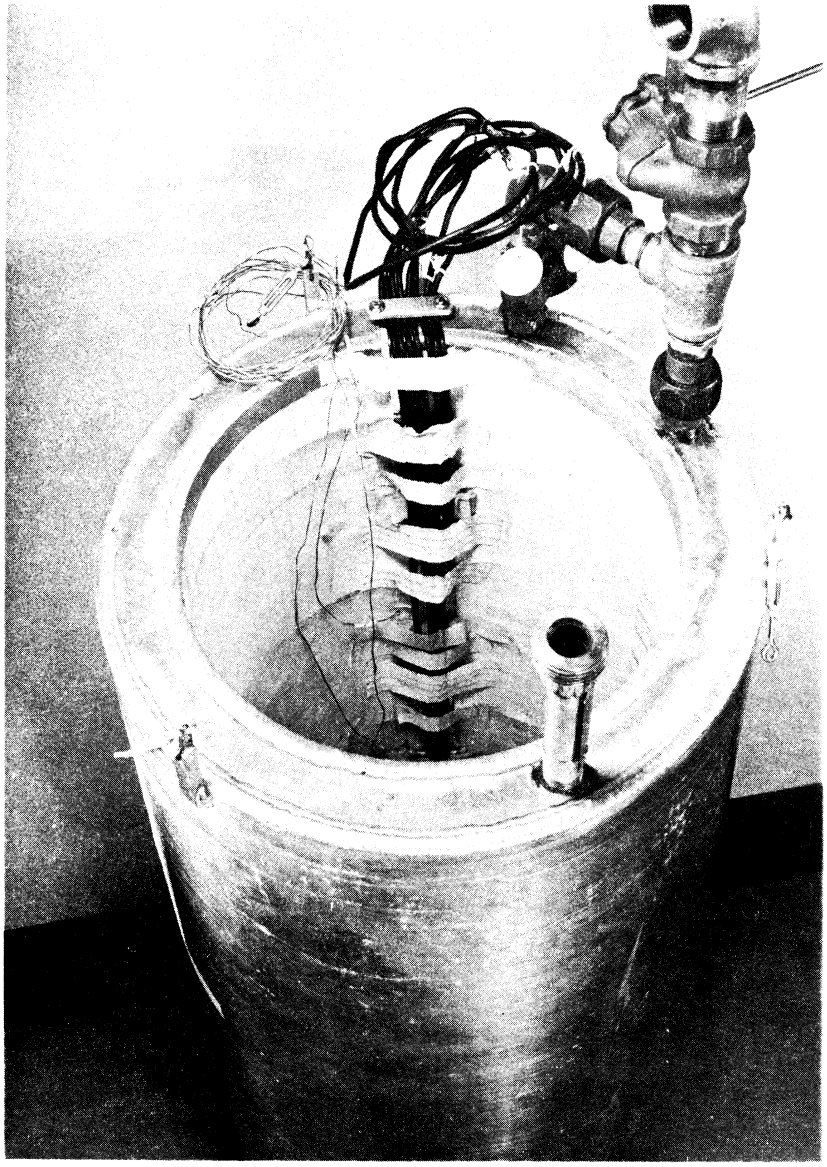

Fig. 6. Photograph of annular container.

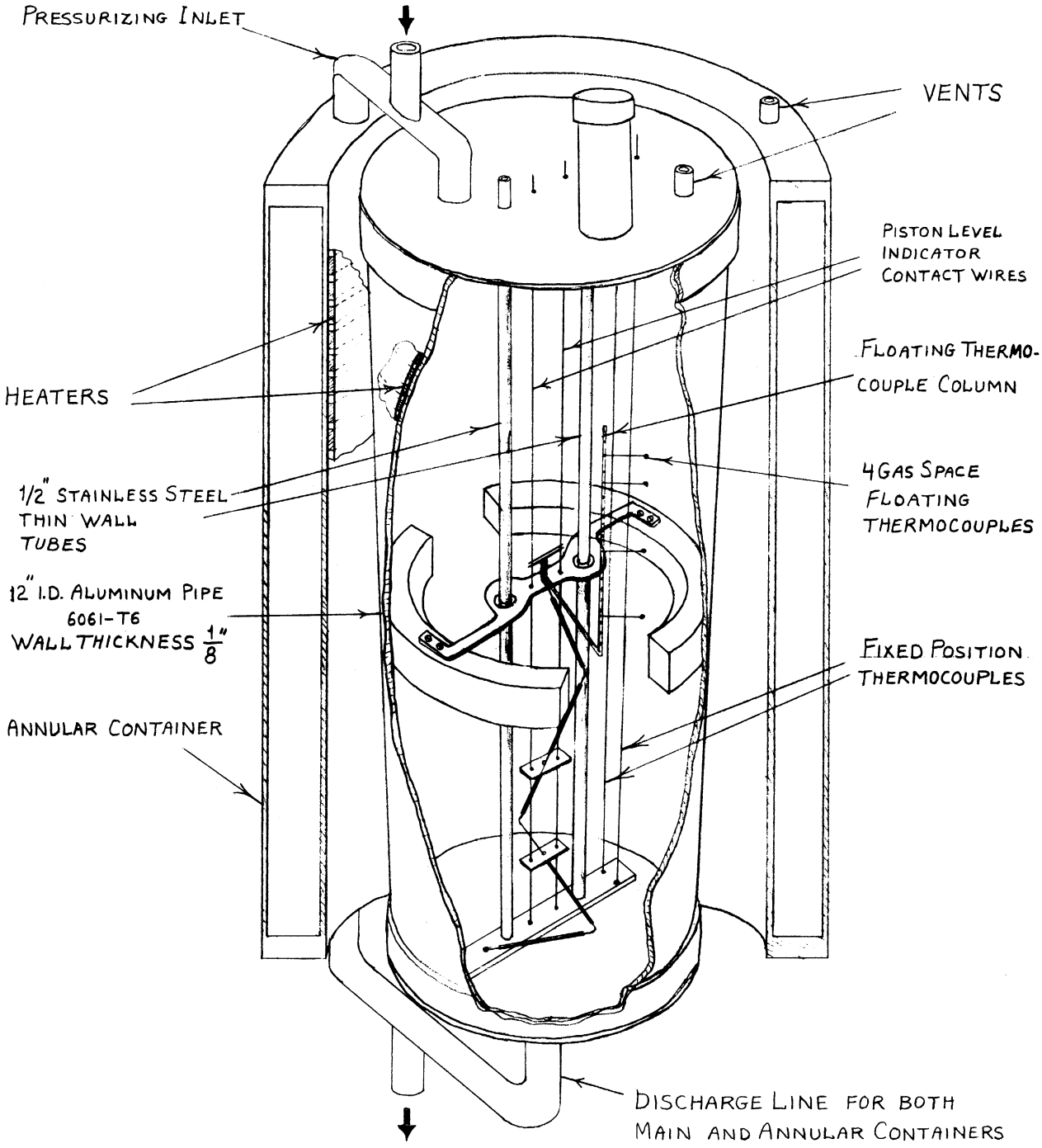

Fig. 7. Sectional view of main and annular containers.

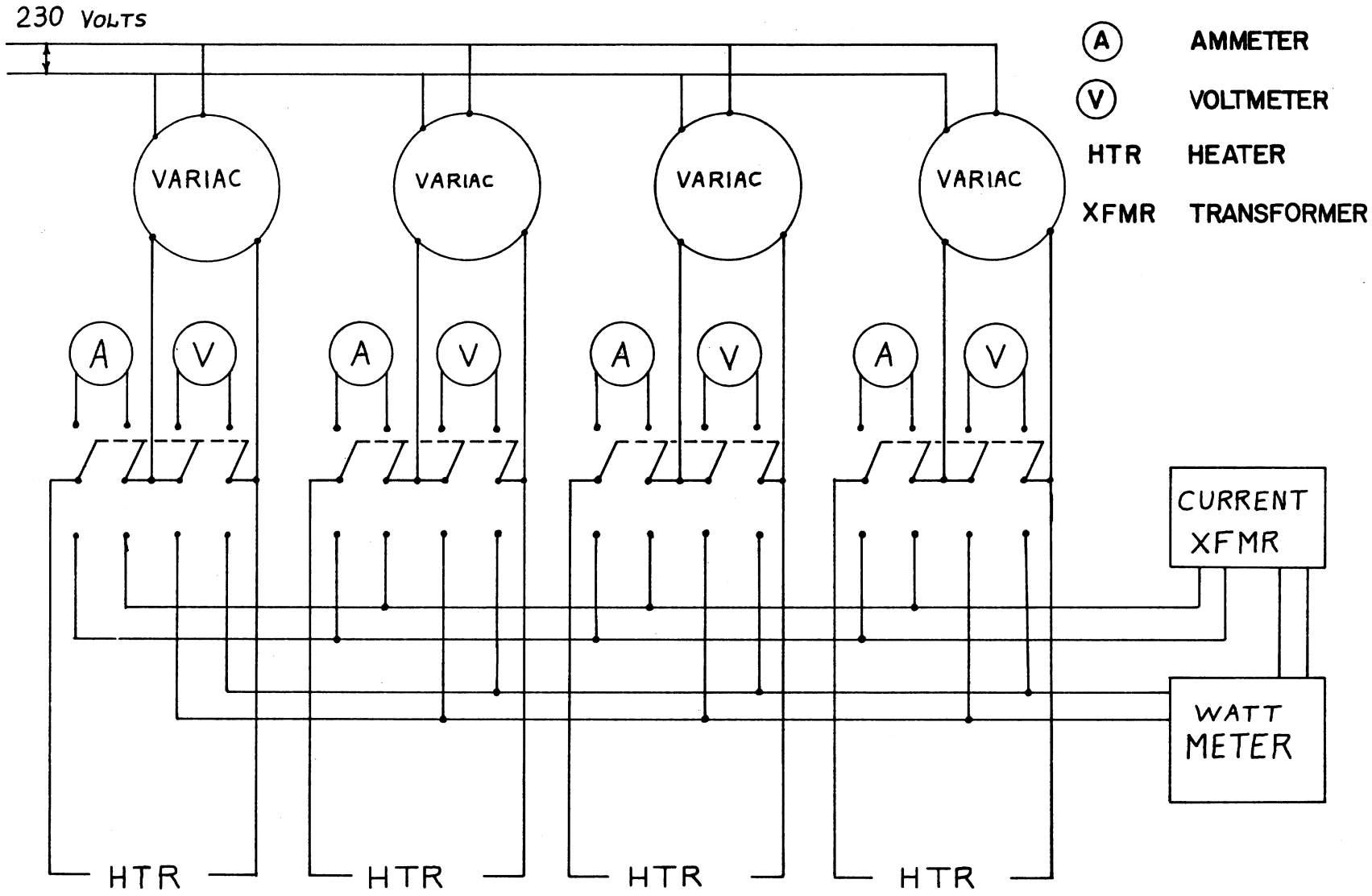

Fig. 8. Resistance heater wiring diagram.

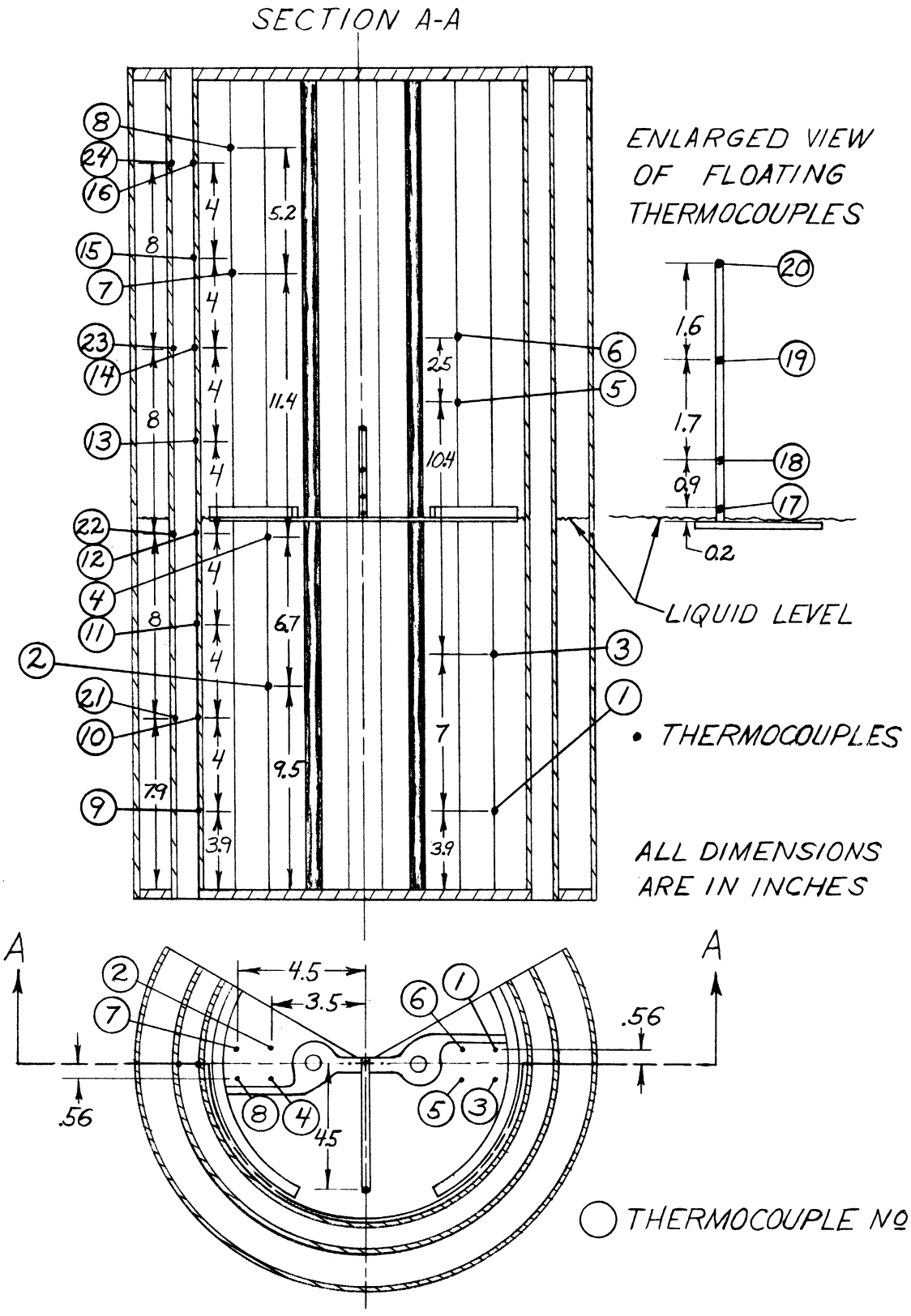

Fig. 9. Thermocouple locations in system.

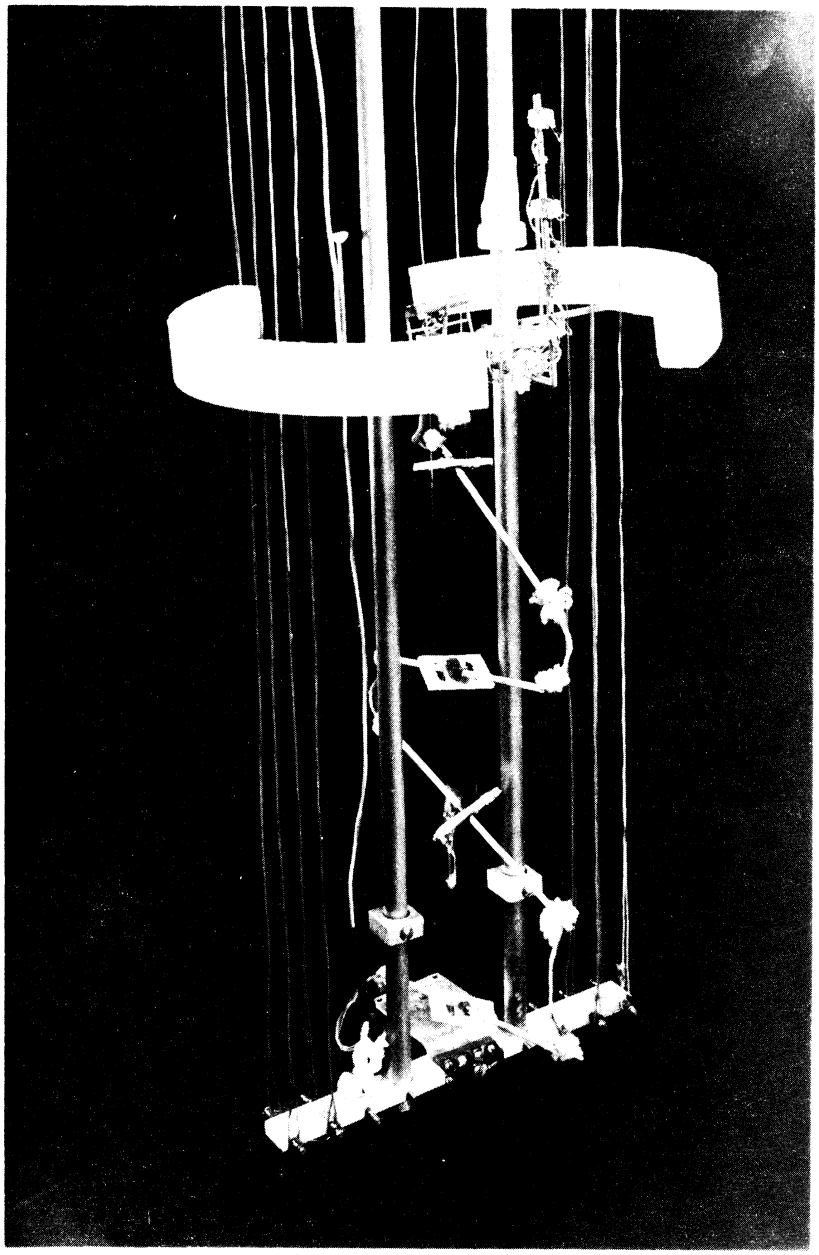

Fig. 10. Photograph showing level indicator and floating thermocouple assembly.

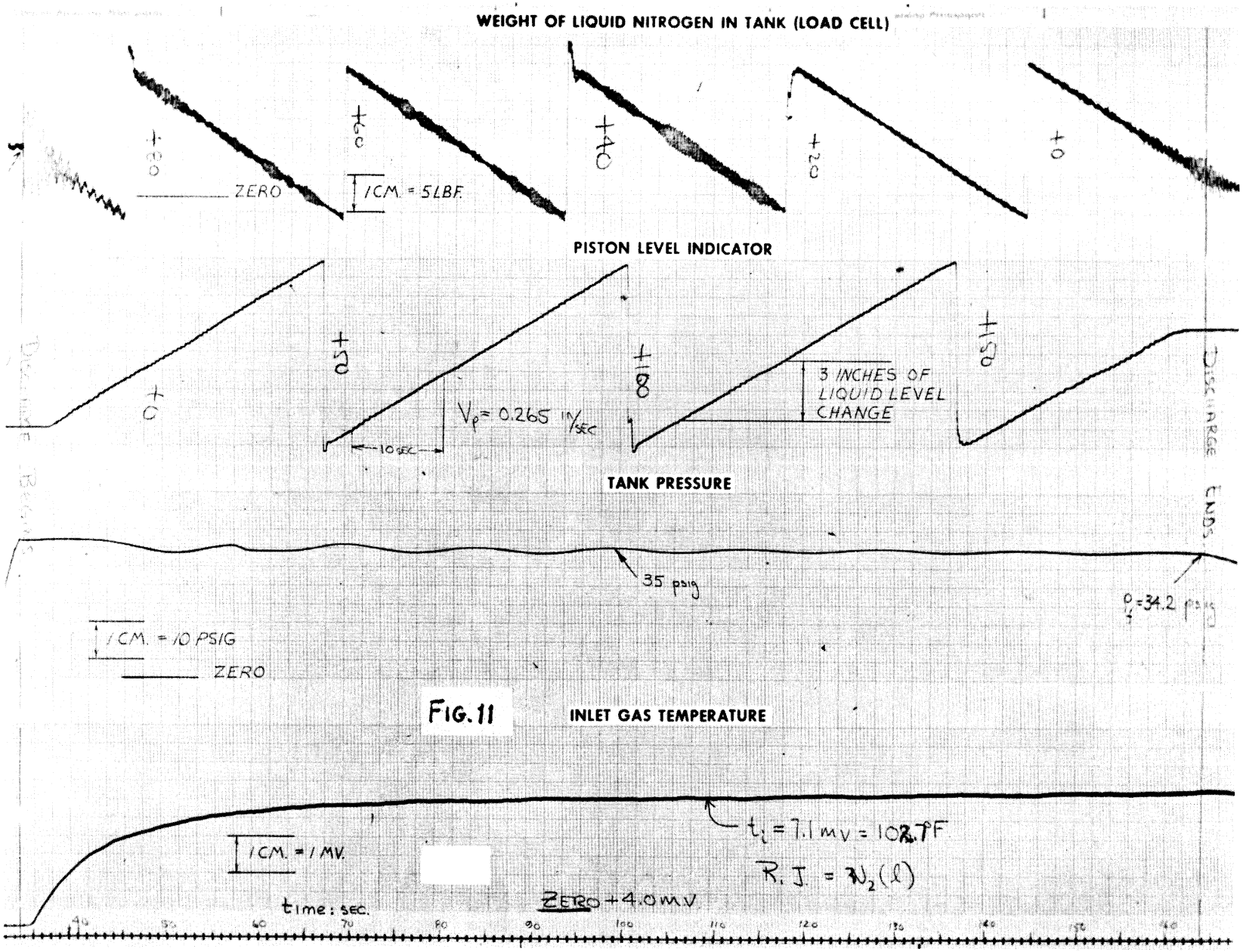

FIG. 11

Fig. 11. A typical Sanborn oscillographic record of a run.

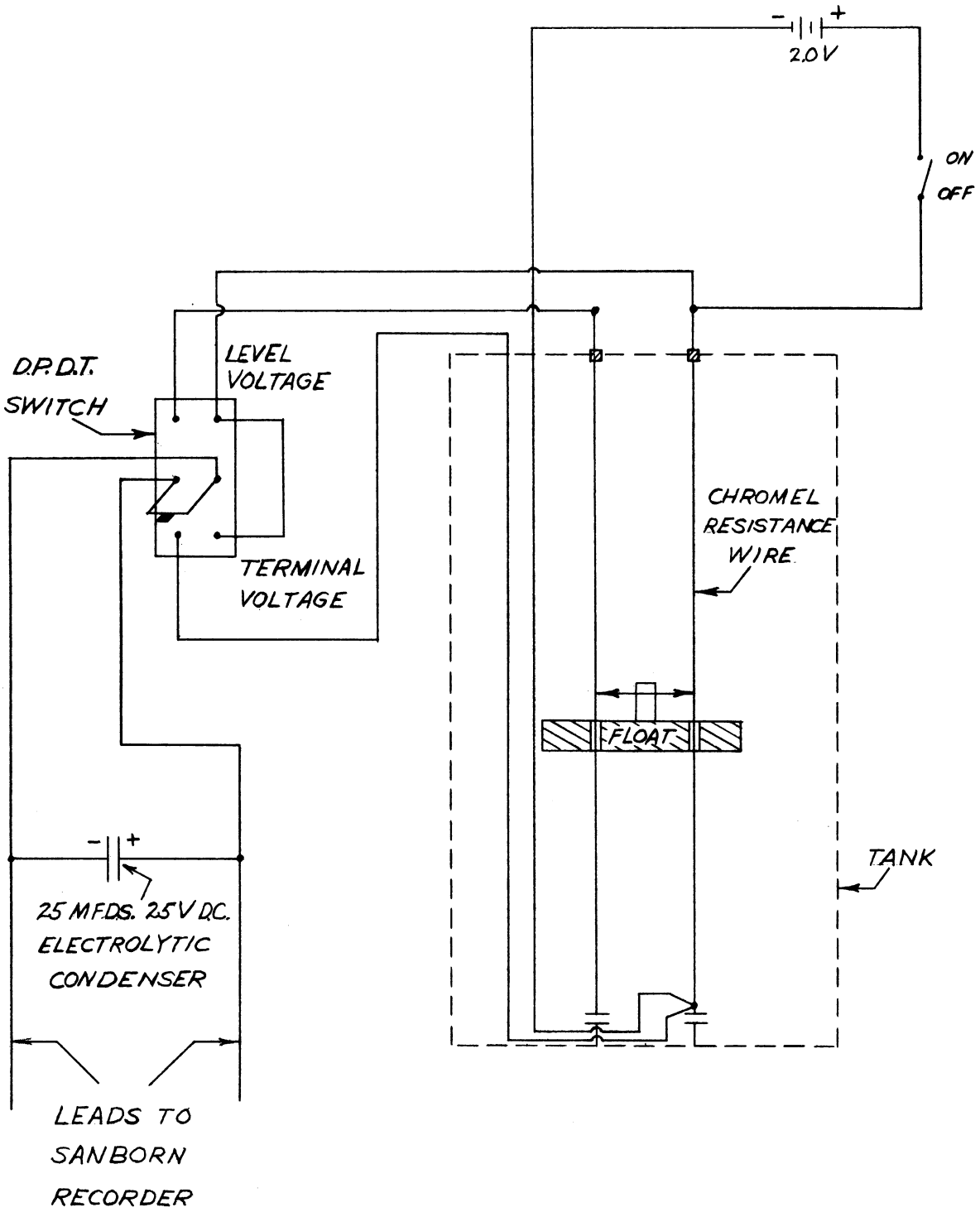

Fig. 12. Wiring diagram of liquid level indicator.

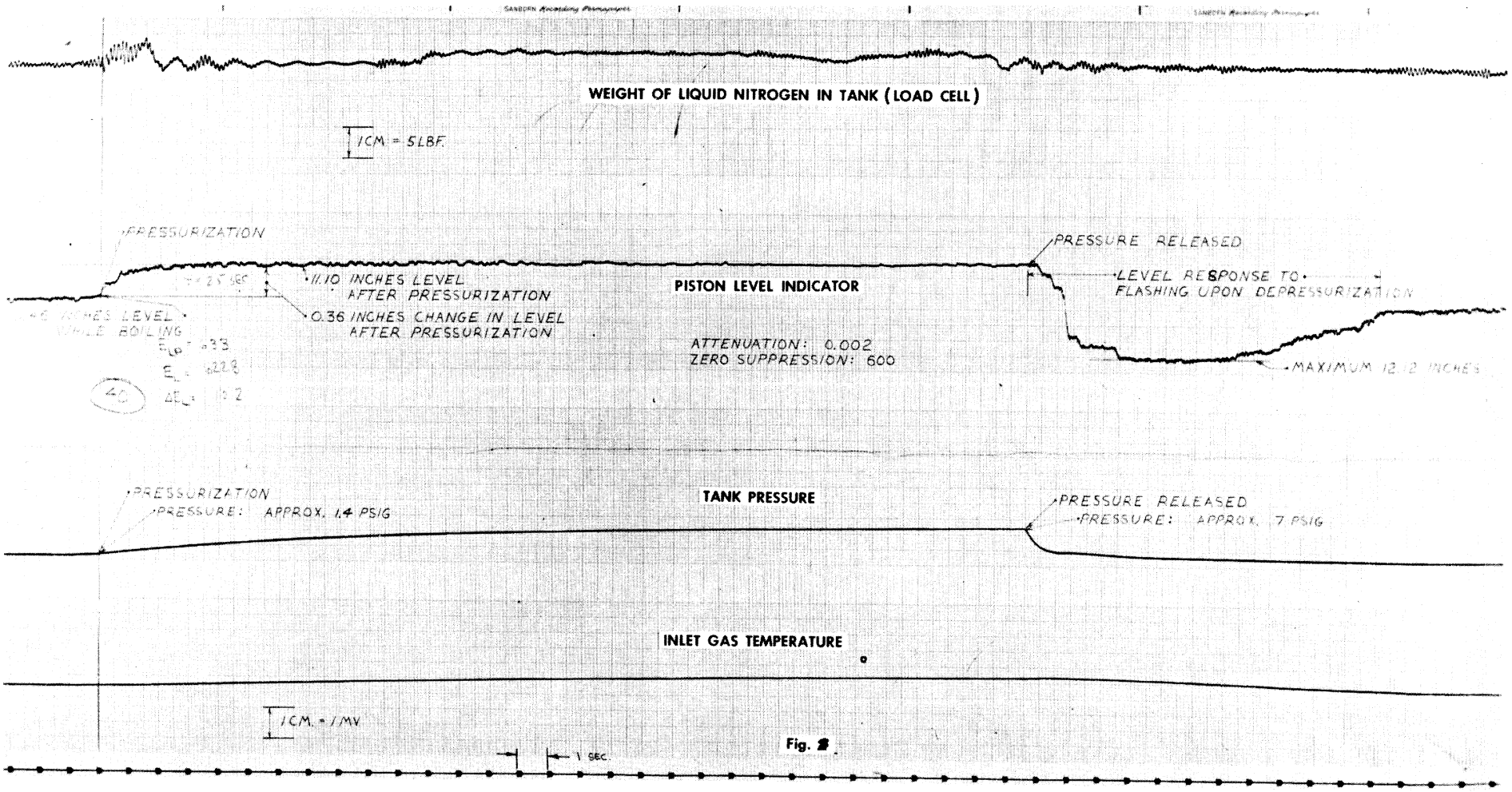

Fig. 13. Sanborn record of liquid level during pressurization and de-pressurization.

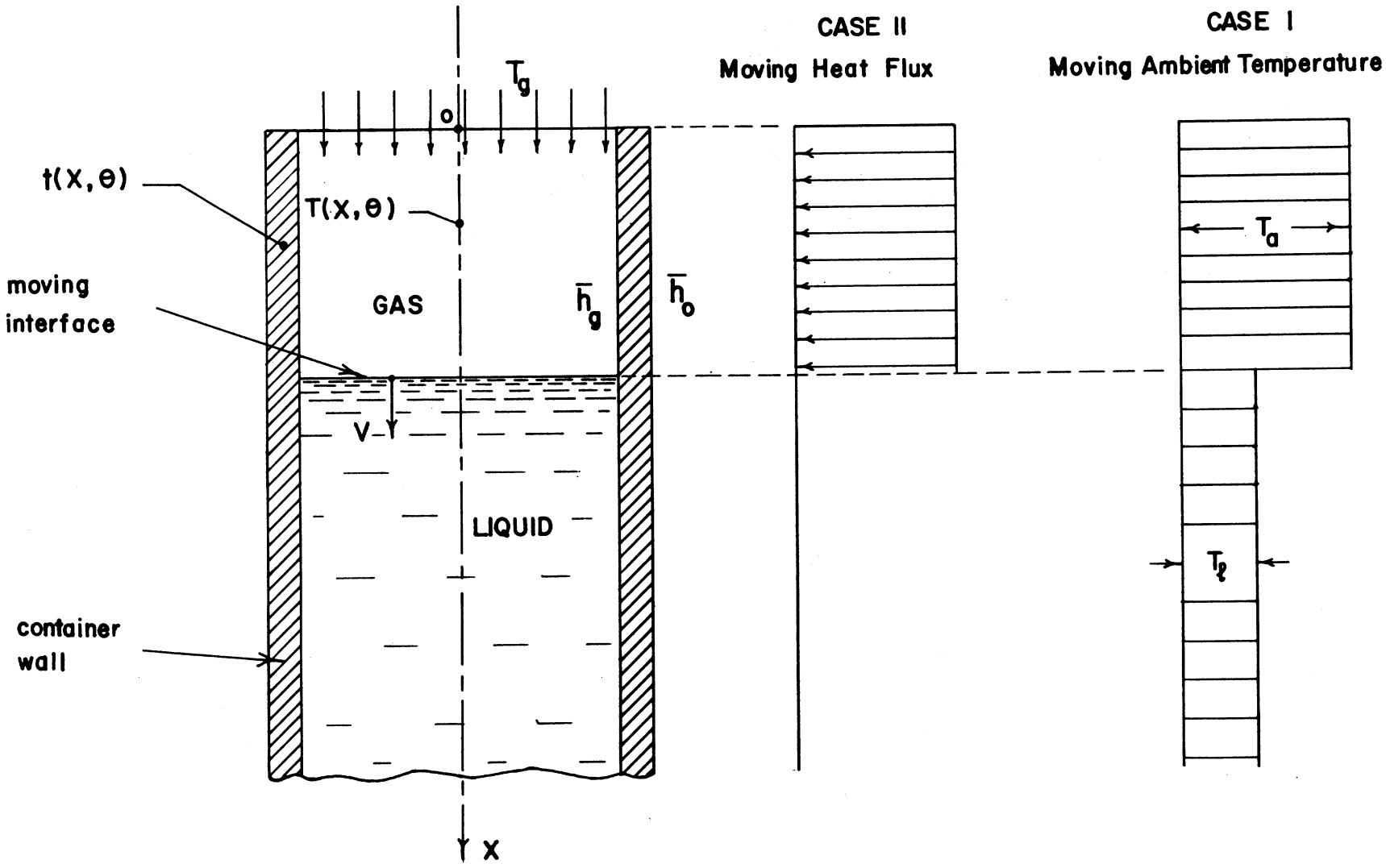

Fig. 14. Analytical model.

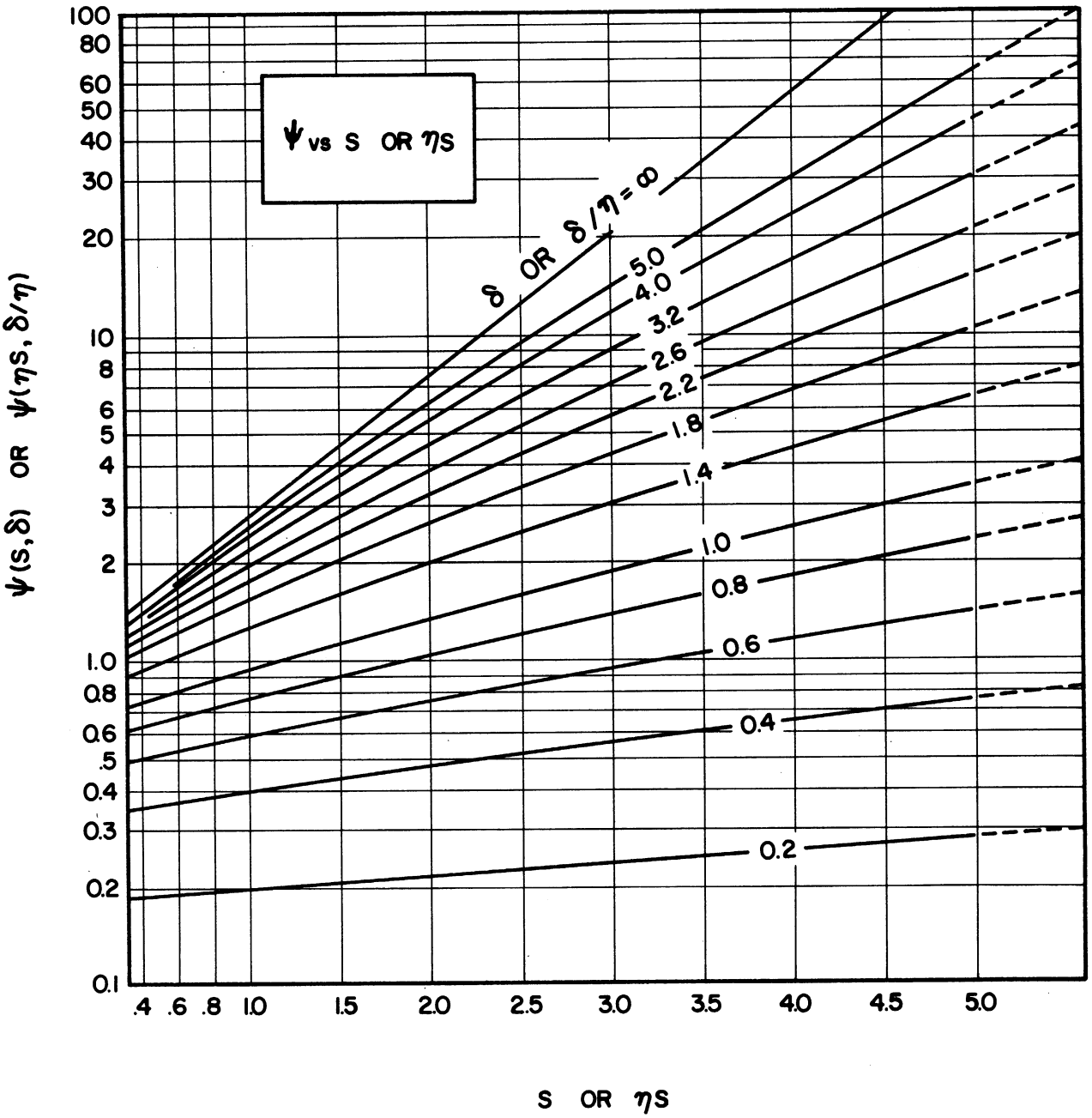

Fig. 15. The function $\psi(s,\delta)$ or $\psi(\eta s,\frac{\delta}{\eta})$.

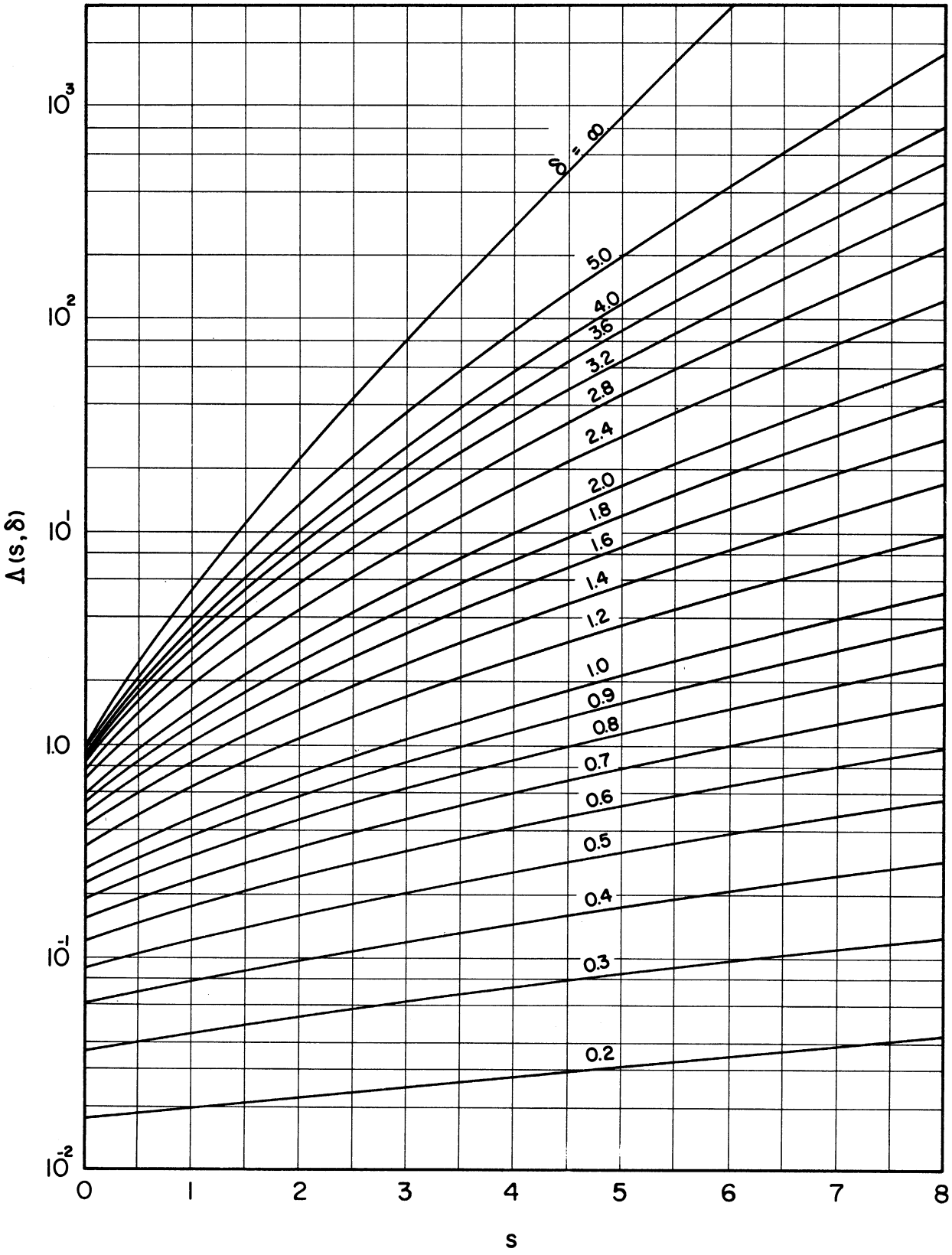

Fig. 16. The function $\Lambda(s,\delta)$.

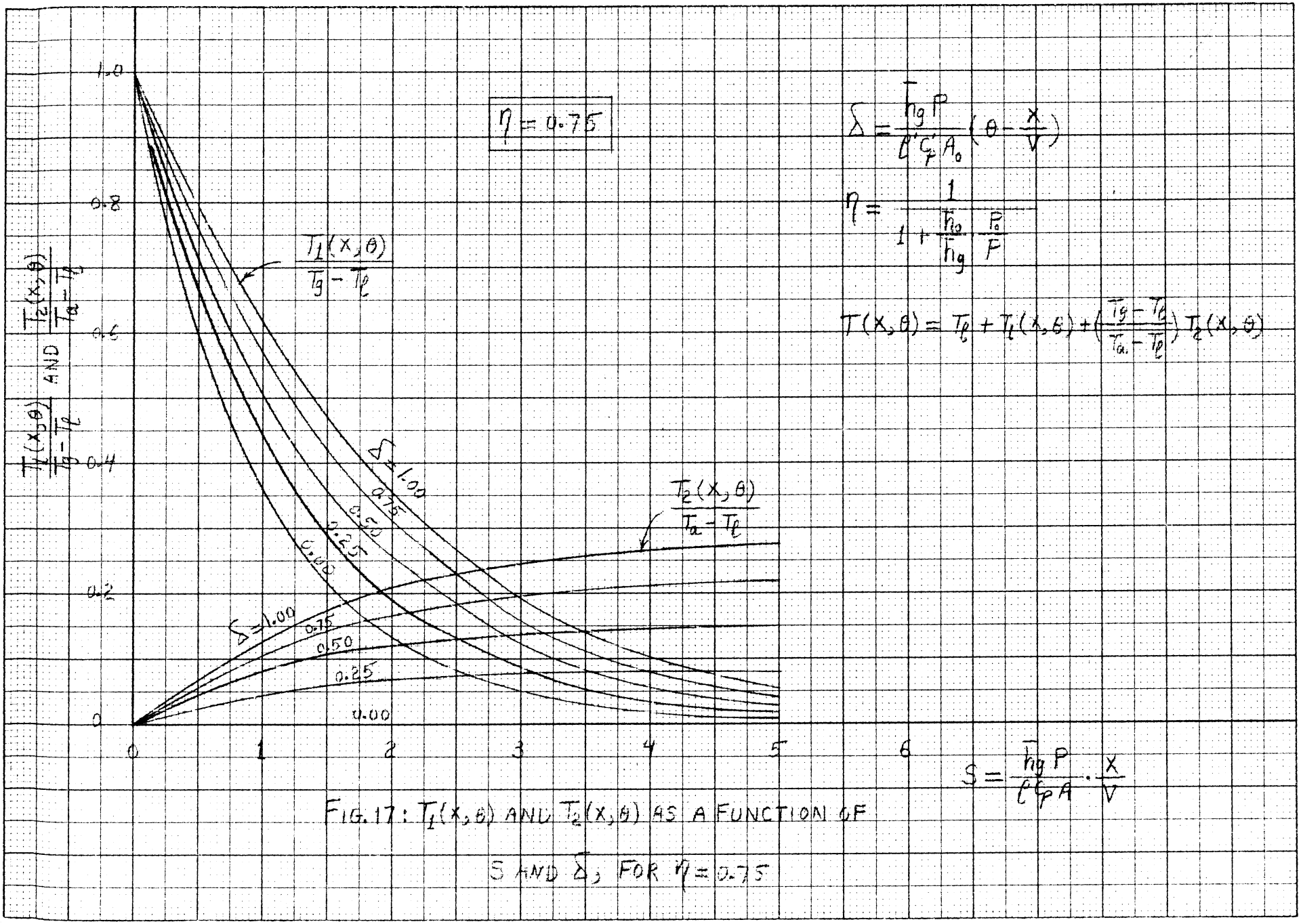

FIG. 17 : $T_1(X,\theta)$ AND $T_2(X,\theta)$ AS A FUNCTION OF S AND Δ, FOR $\eta = 0.75$

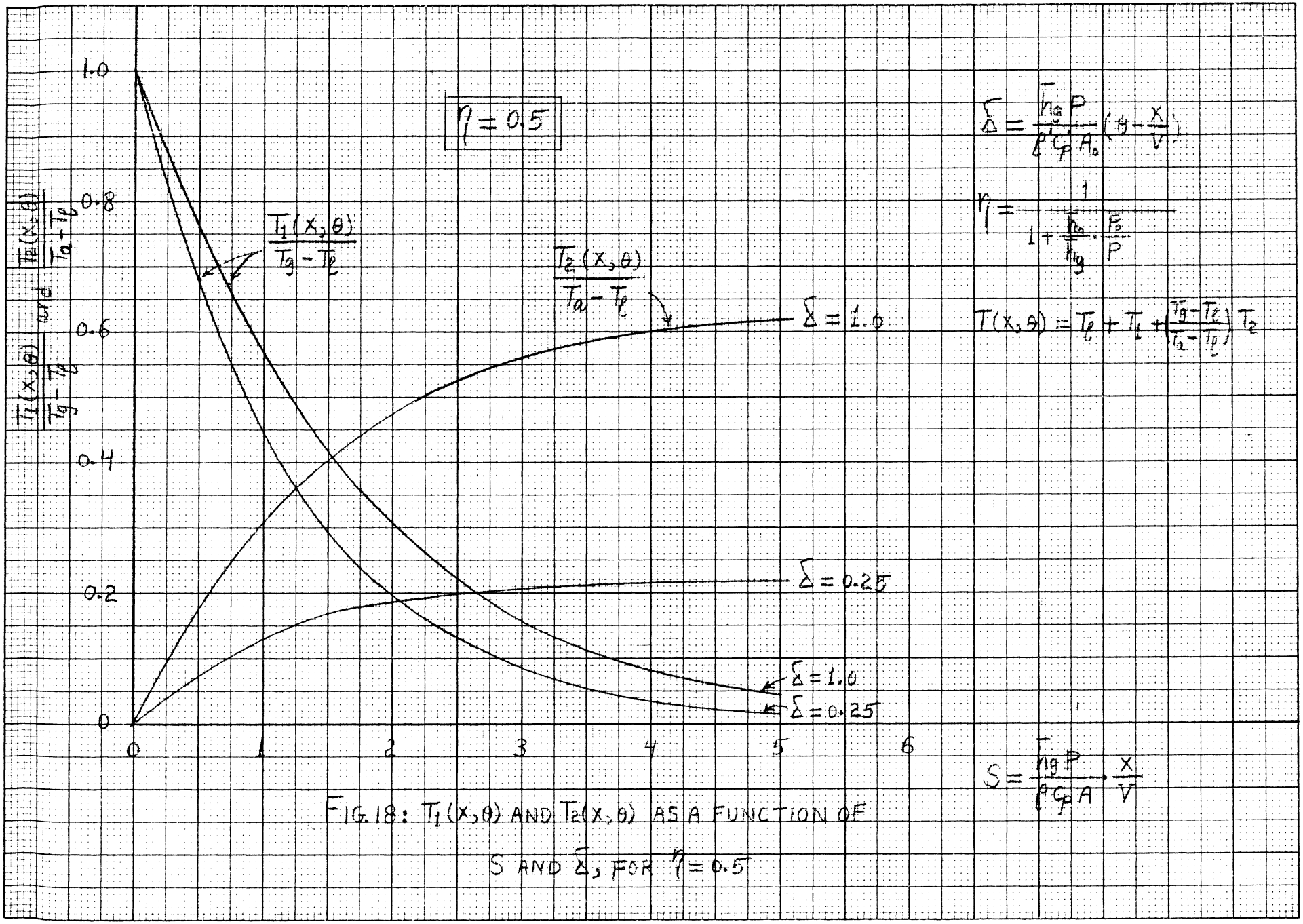

FIG. 18: $T_1(X,\theta)$ AND $T_2(X,\theta)$ AS A FUNCTION OF S AND $\bar{\Delta}$, FOR $\eta = 0.5$

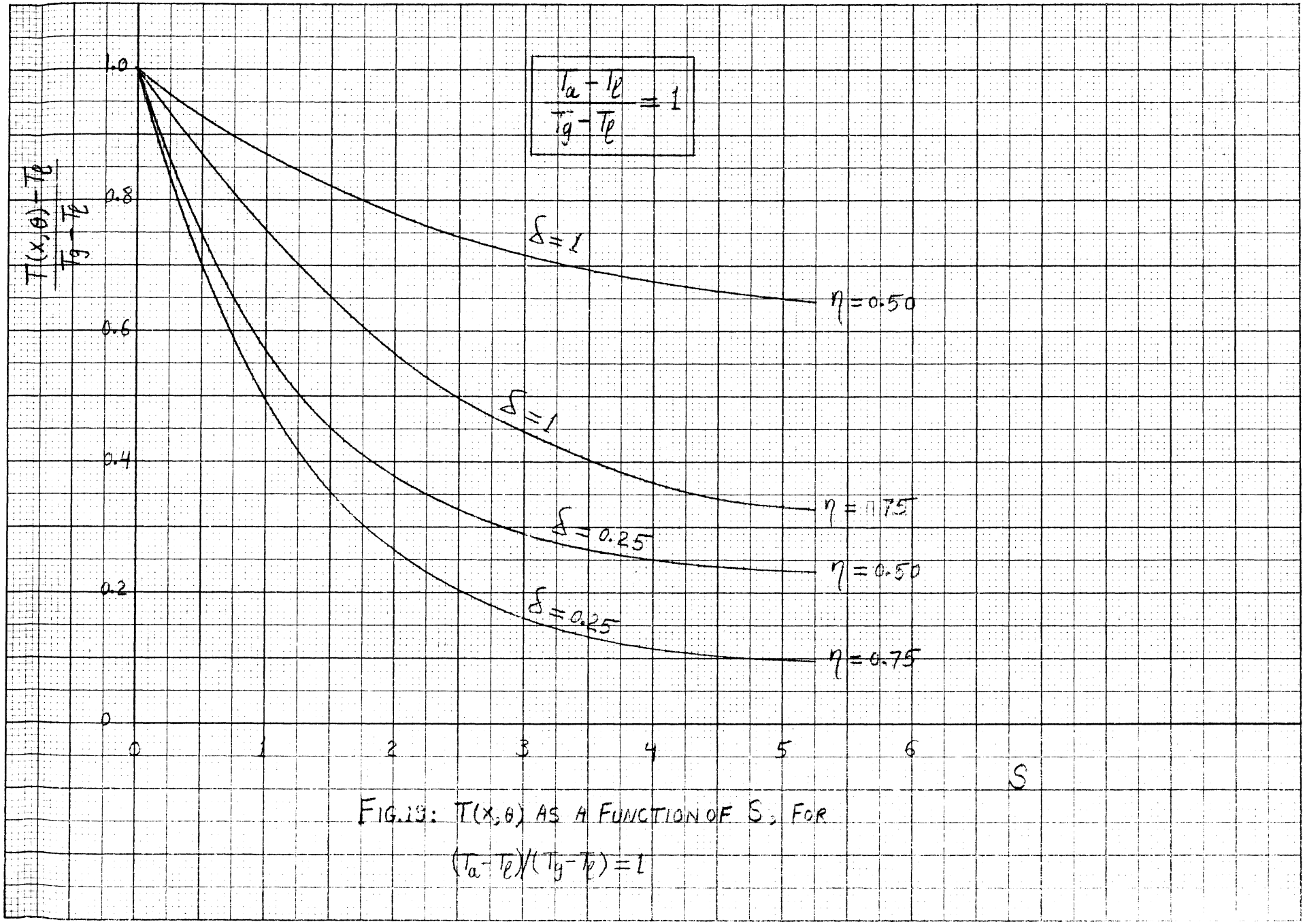

FIG. 13: $T(X,\theta)$ AS A FUNCTION OF S, FOR $(T_a - T_\ell)/(T_g - T_\ell) = 1$

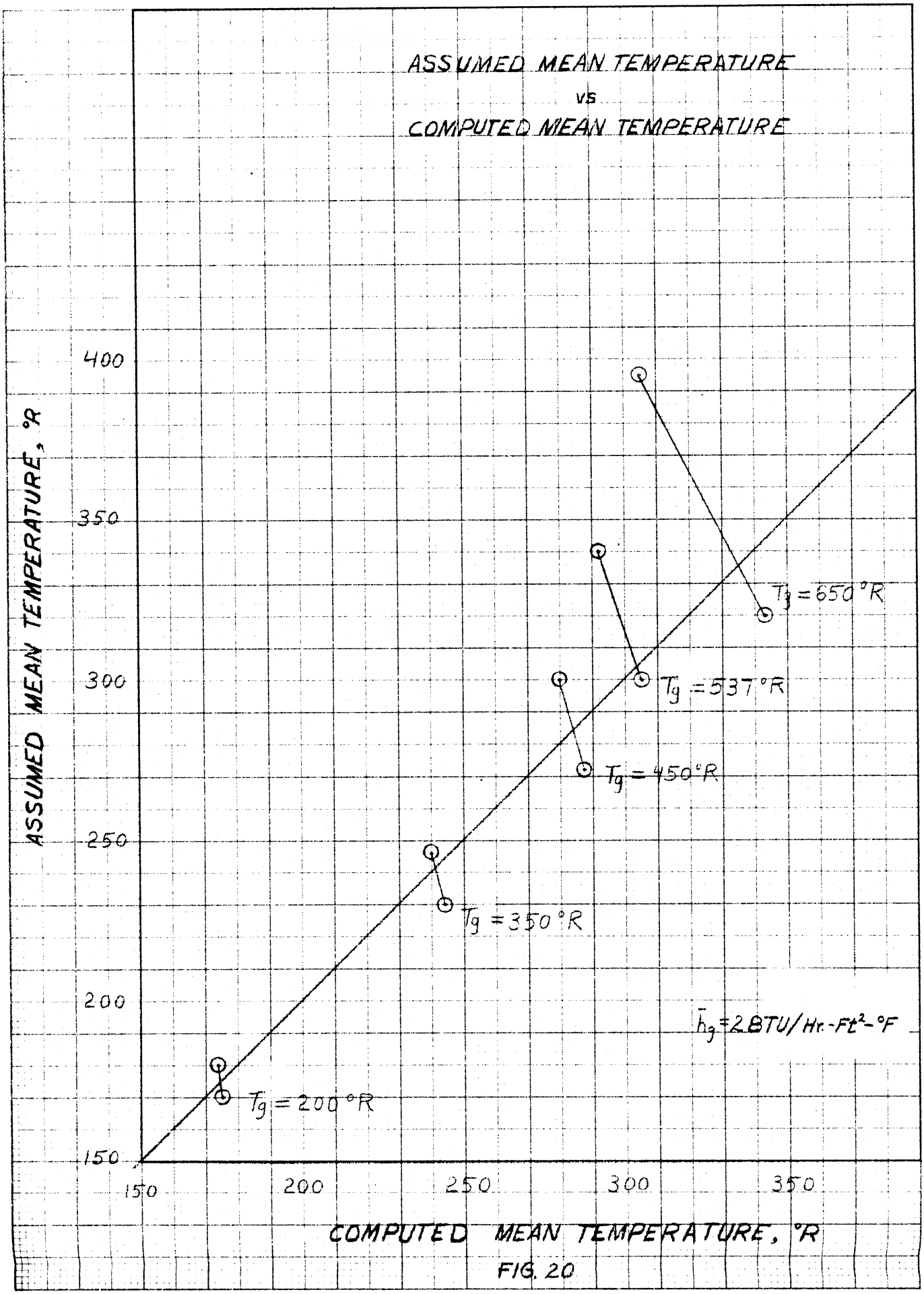
ASSUMED MEAN TEMPERATURE
VS
COMPUTED MEAN TEMPERATURE
ASSUMED MEAN TEMPERATURE, °R
400
350
300
250
200
150
150
200
250
300
350
COMPUTED MEAN TEMPERATURE, °R
$T_g = 650°R$
$T_g = 537°R$
$T_g = 450°R$
$T_g = 350°R$
$T_g = 200°R$
$\bar{h}_g = 2$ BTU/Hr-Ft²-°F

FIG. 20

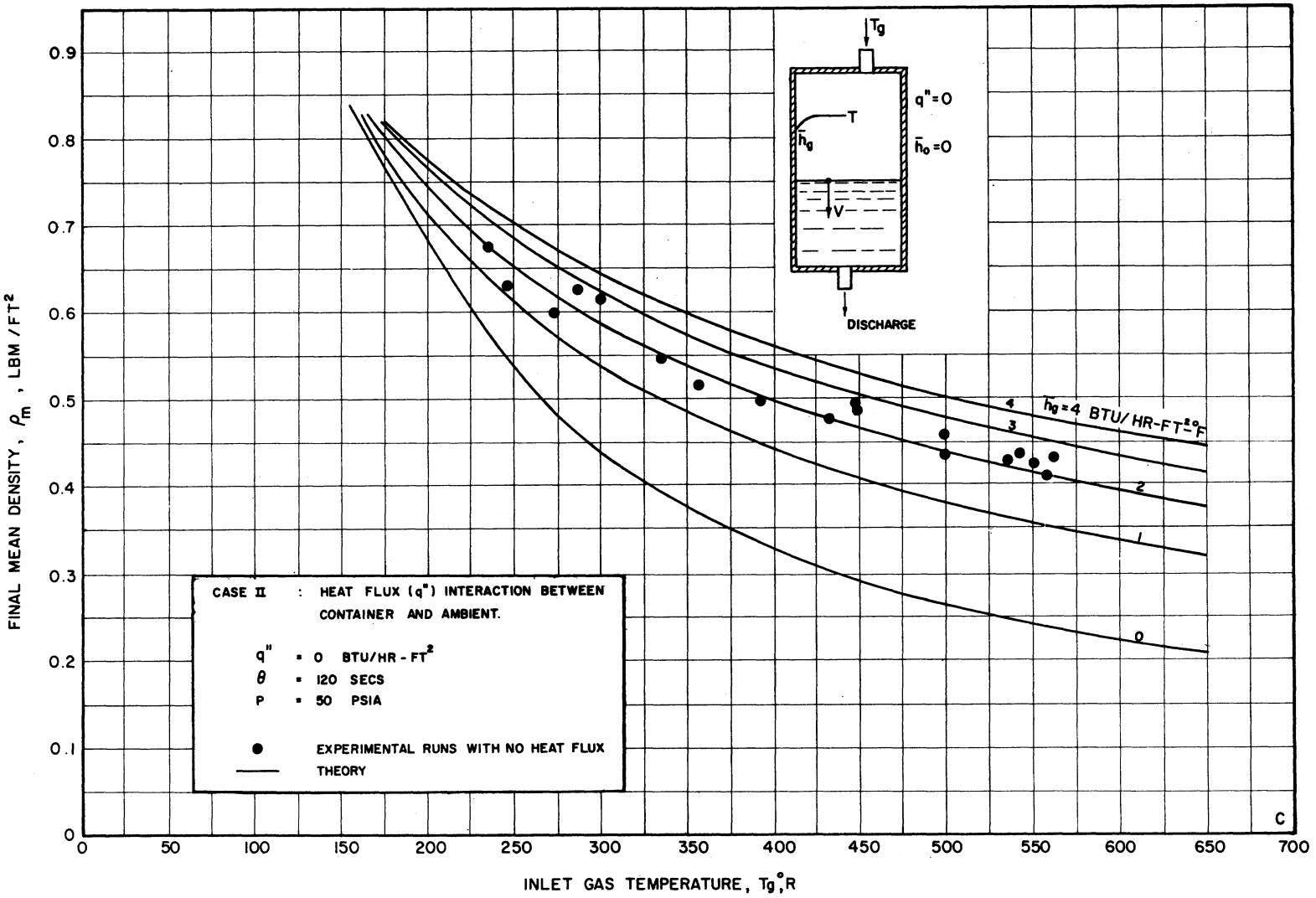

Fig. 21. Mean density vs. inlet temperature - zero heat flux.

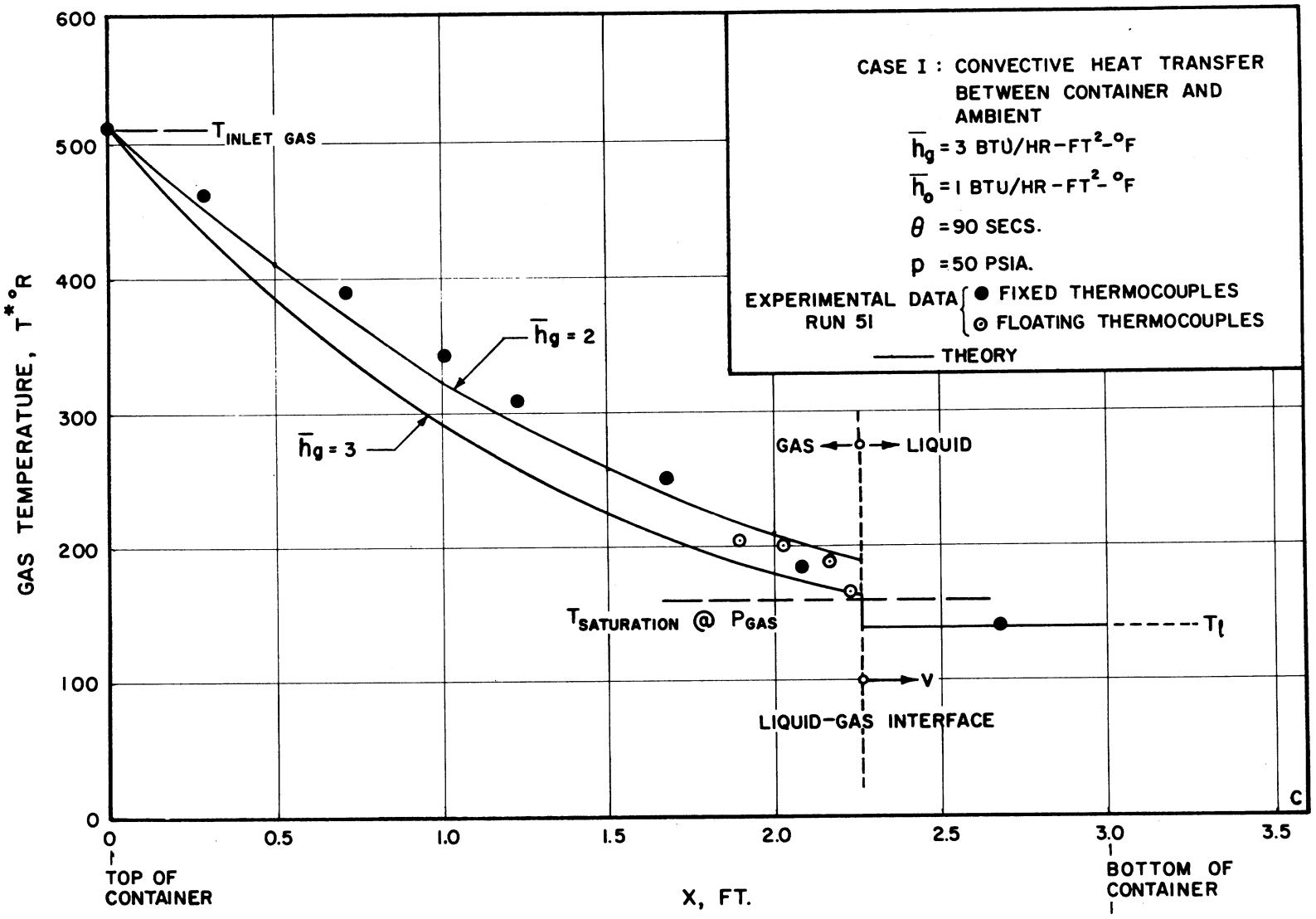

Fig. 23. Gas temperature distribution in container at 90 seconds from discharge.

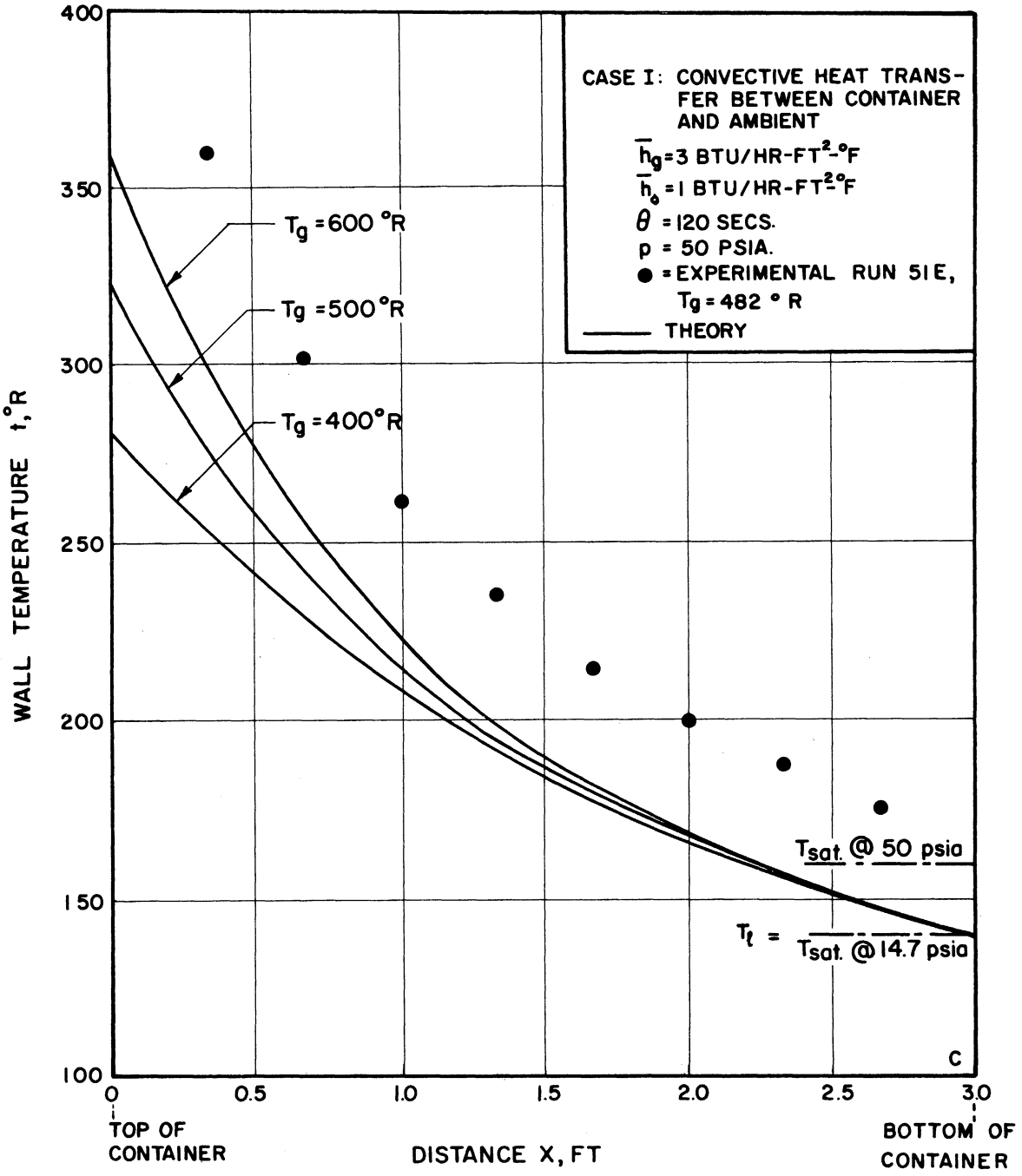

Fig. 24. Wall temperature distribution at end of discharge.

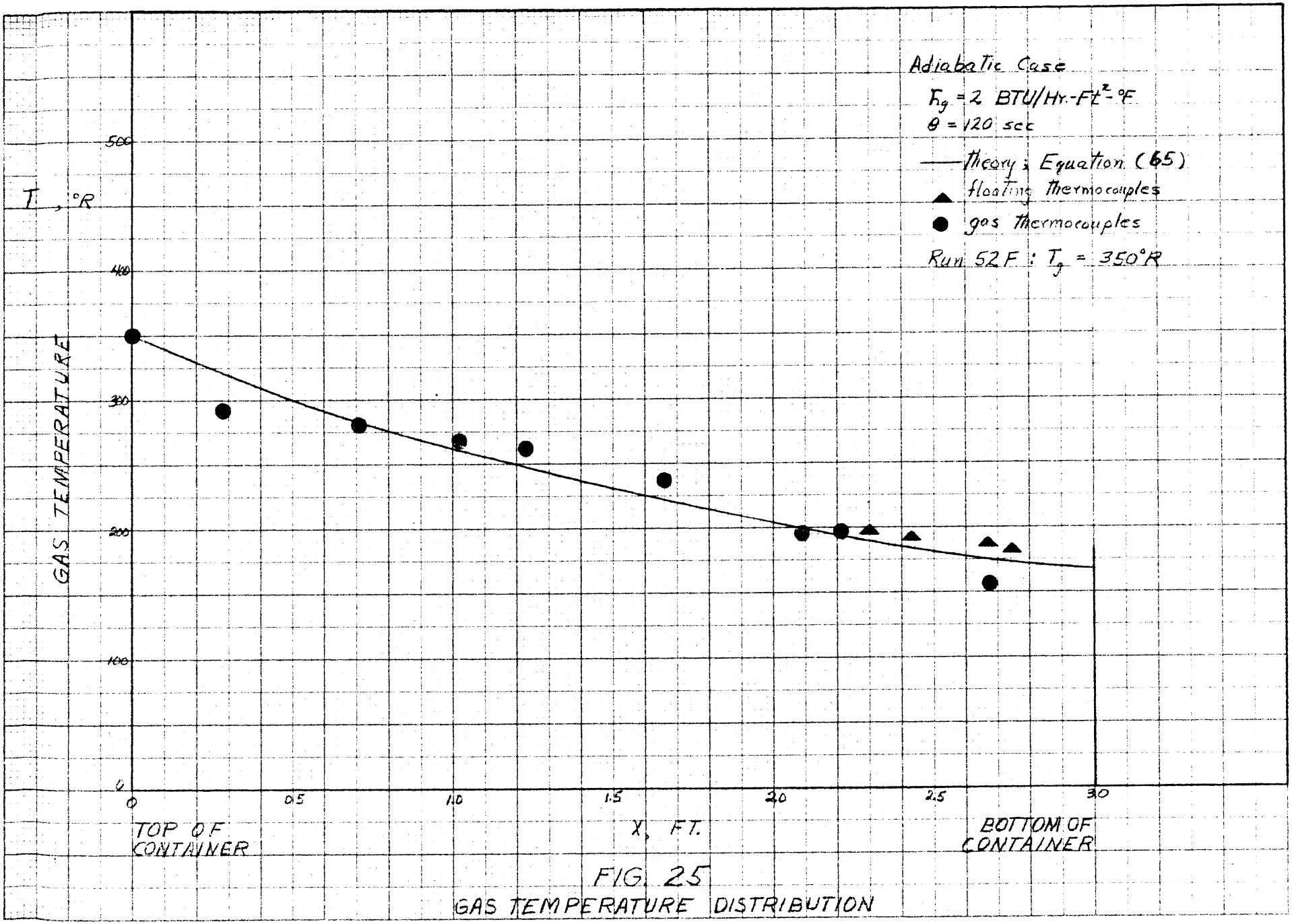

FIG. 25
GAS TEMPERATURE DISTRIBUTION

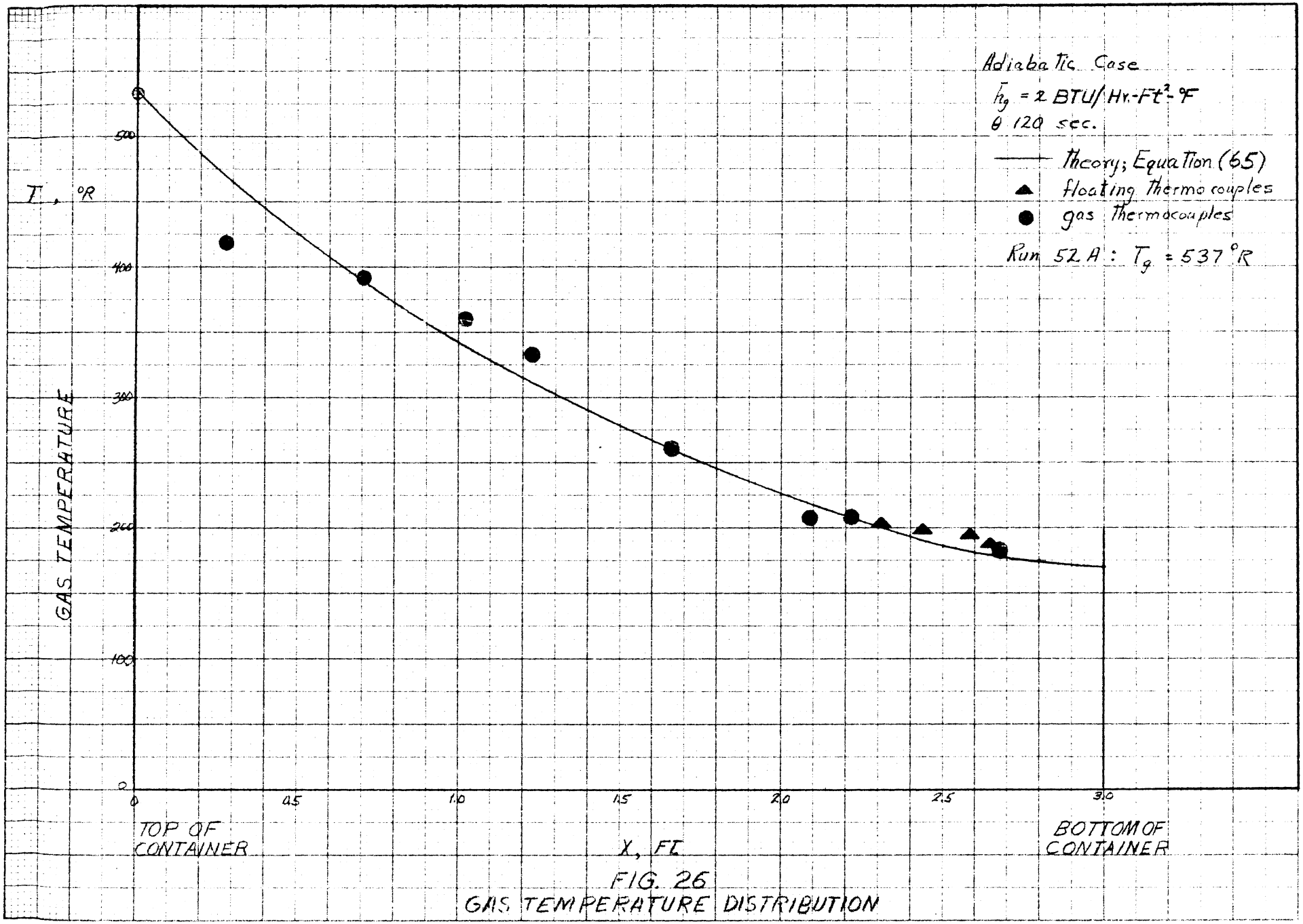

FIG. 26
GAS TEMPERATURE DISTRIBUTION

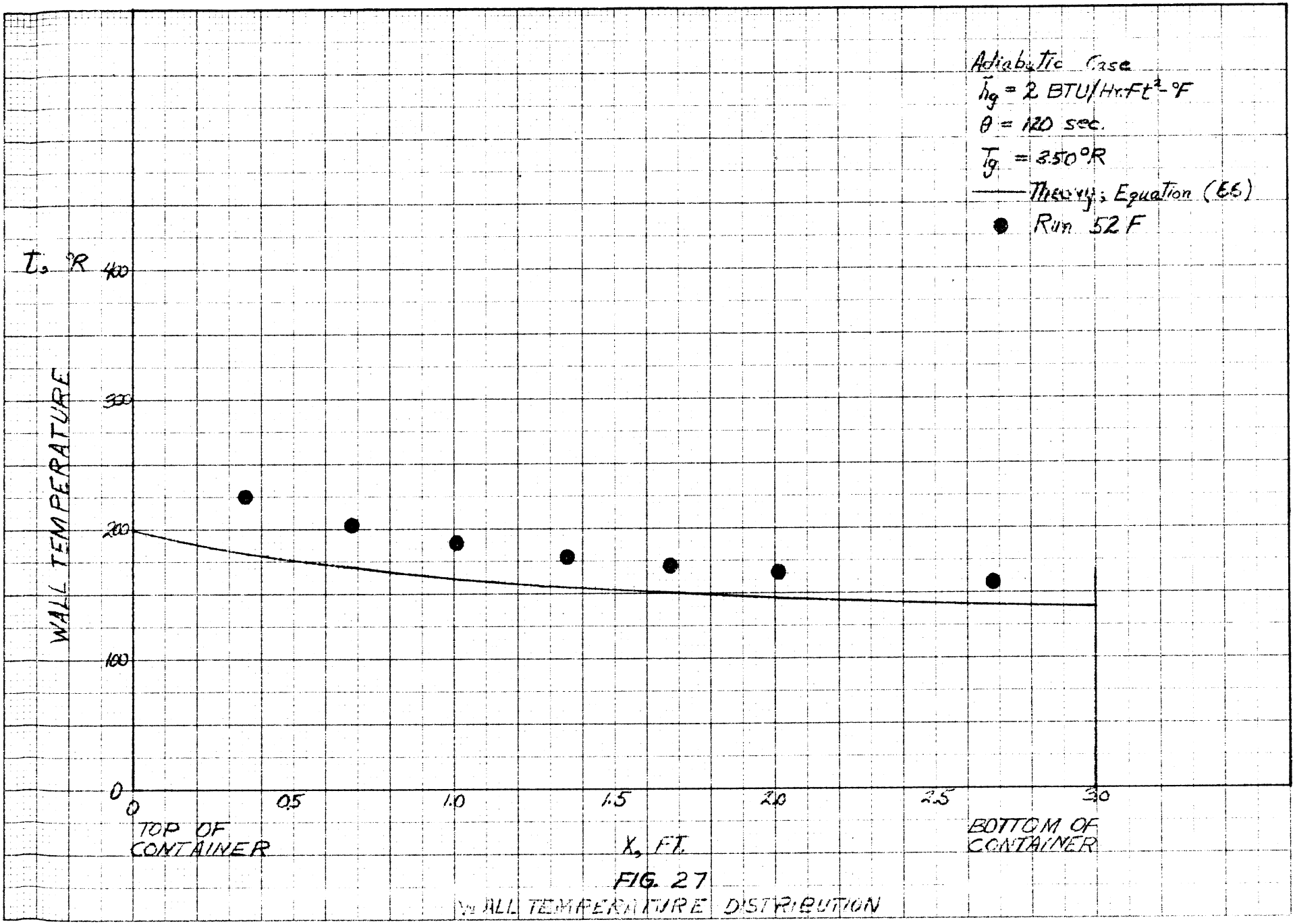

FIG. 27

WALL TEMPERATURE DISTRIBUTION

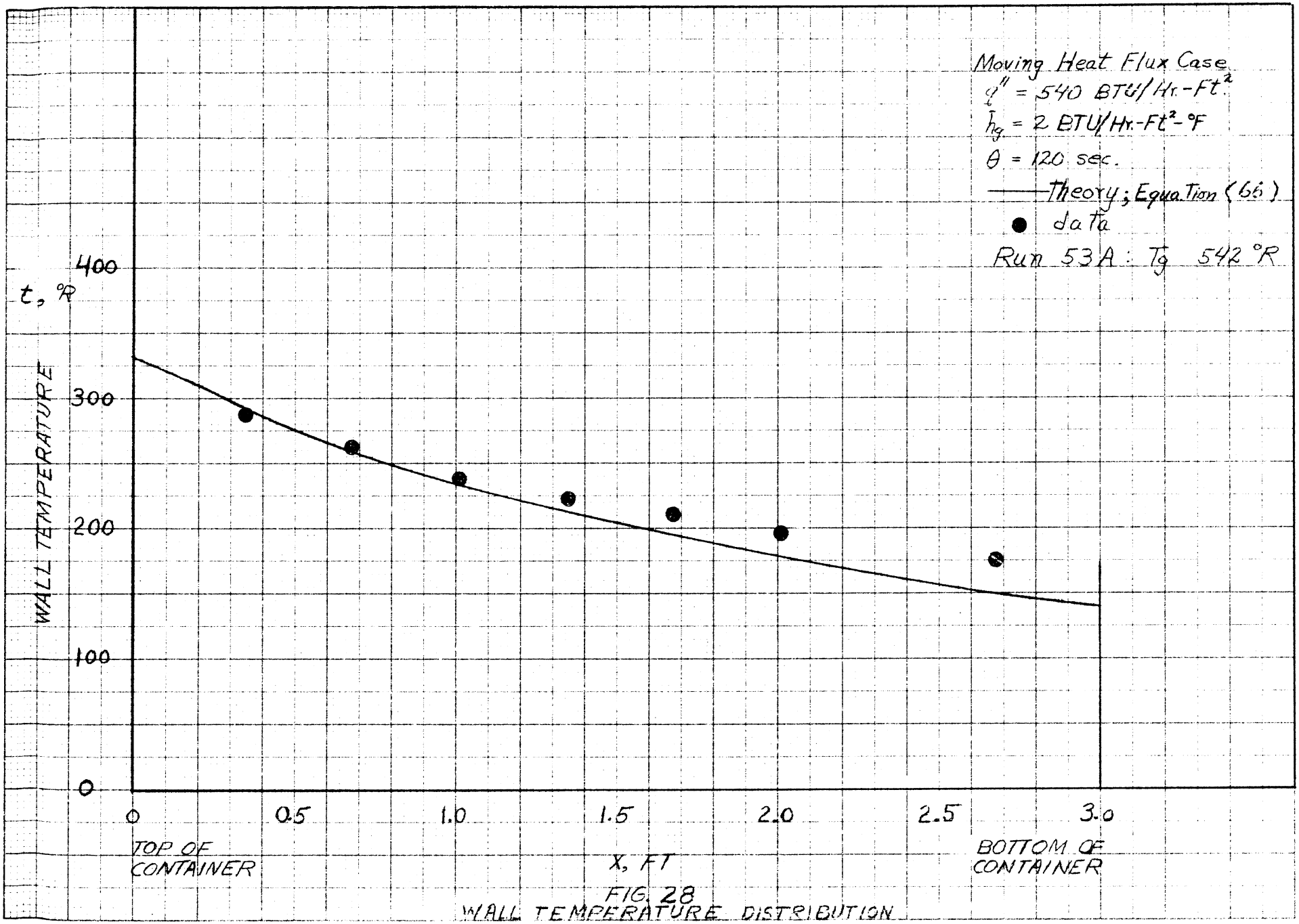

FIG. 28
WALL TEMPERATURE DISTRIBUTION

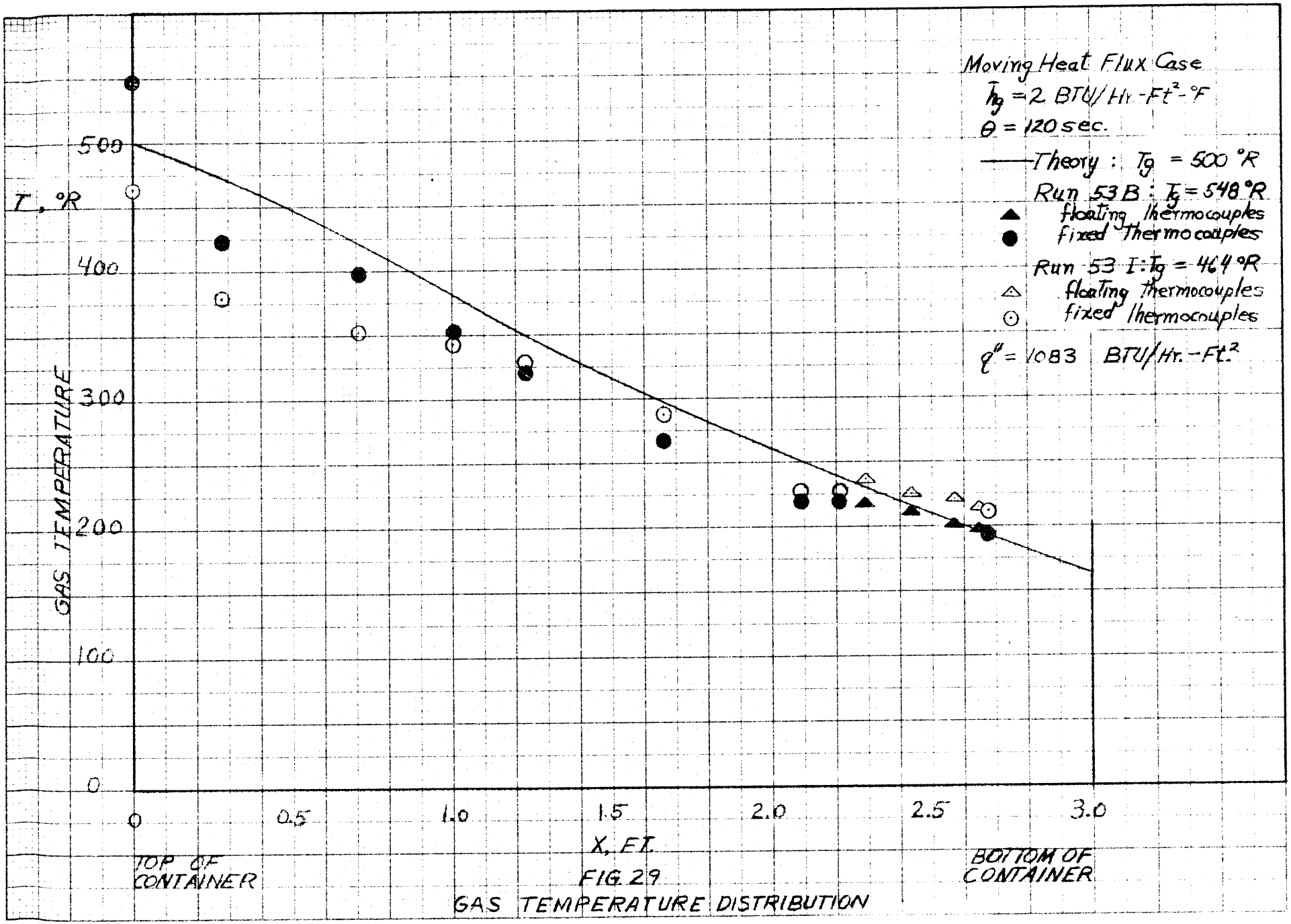

FIG 29
GAS TEMPERATURE DISTRIBUTION

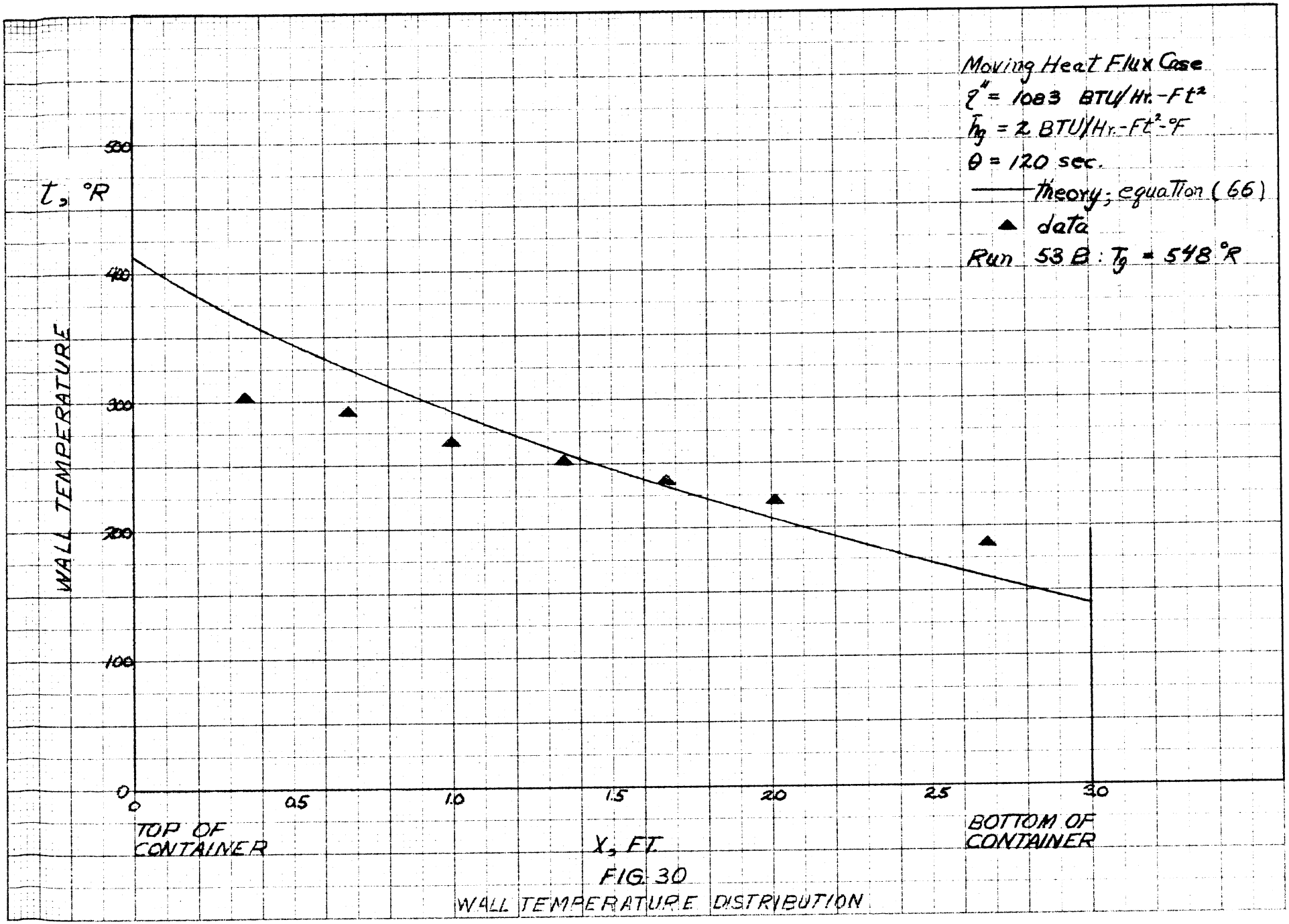

FIG. 30
WALL TEMPERATURE DISTRIBUTION

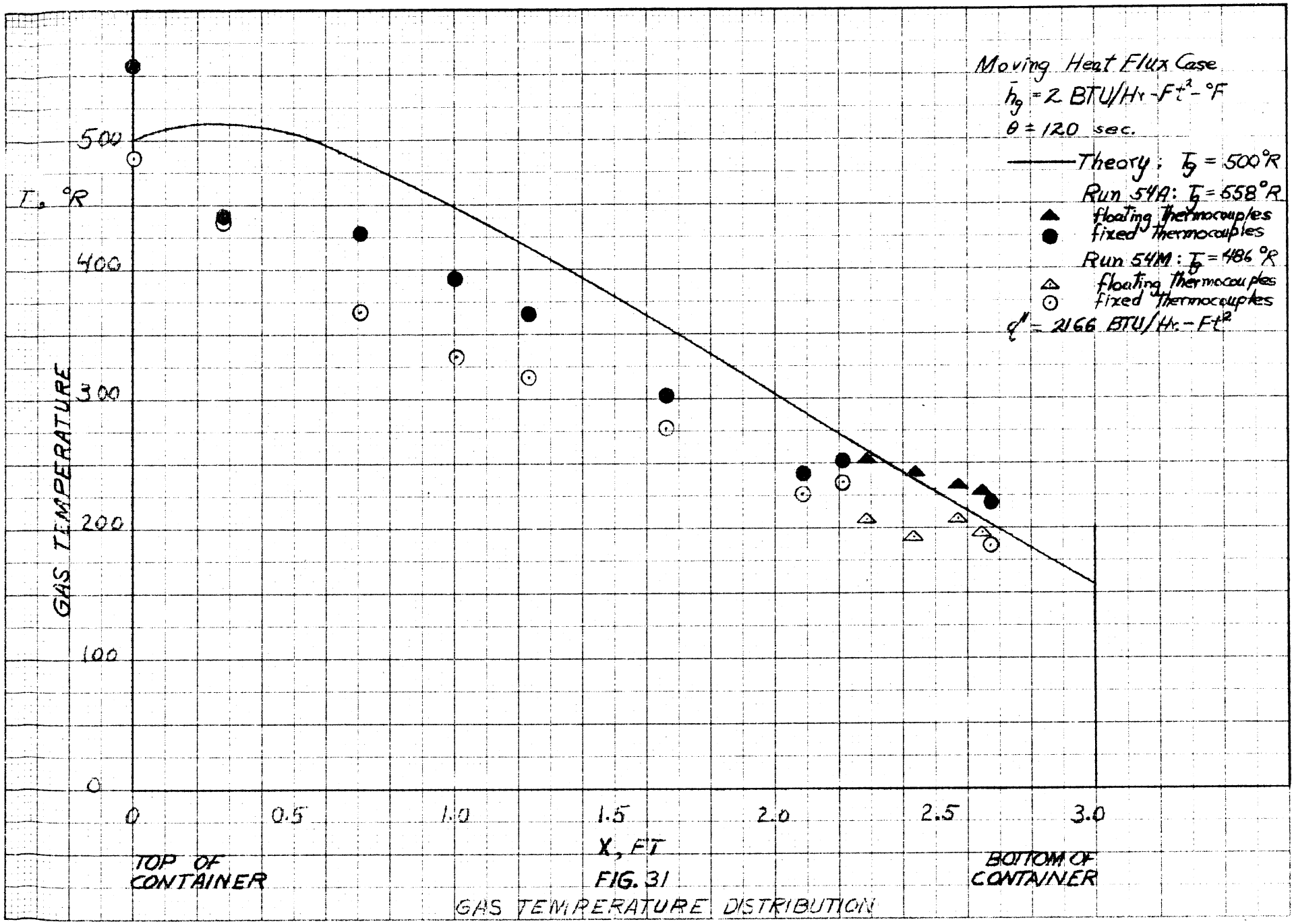

FIG. 31

GAS TEMPERATURE DISTRIBUTION

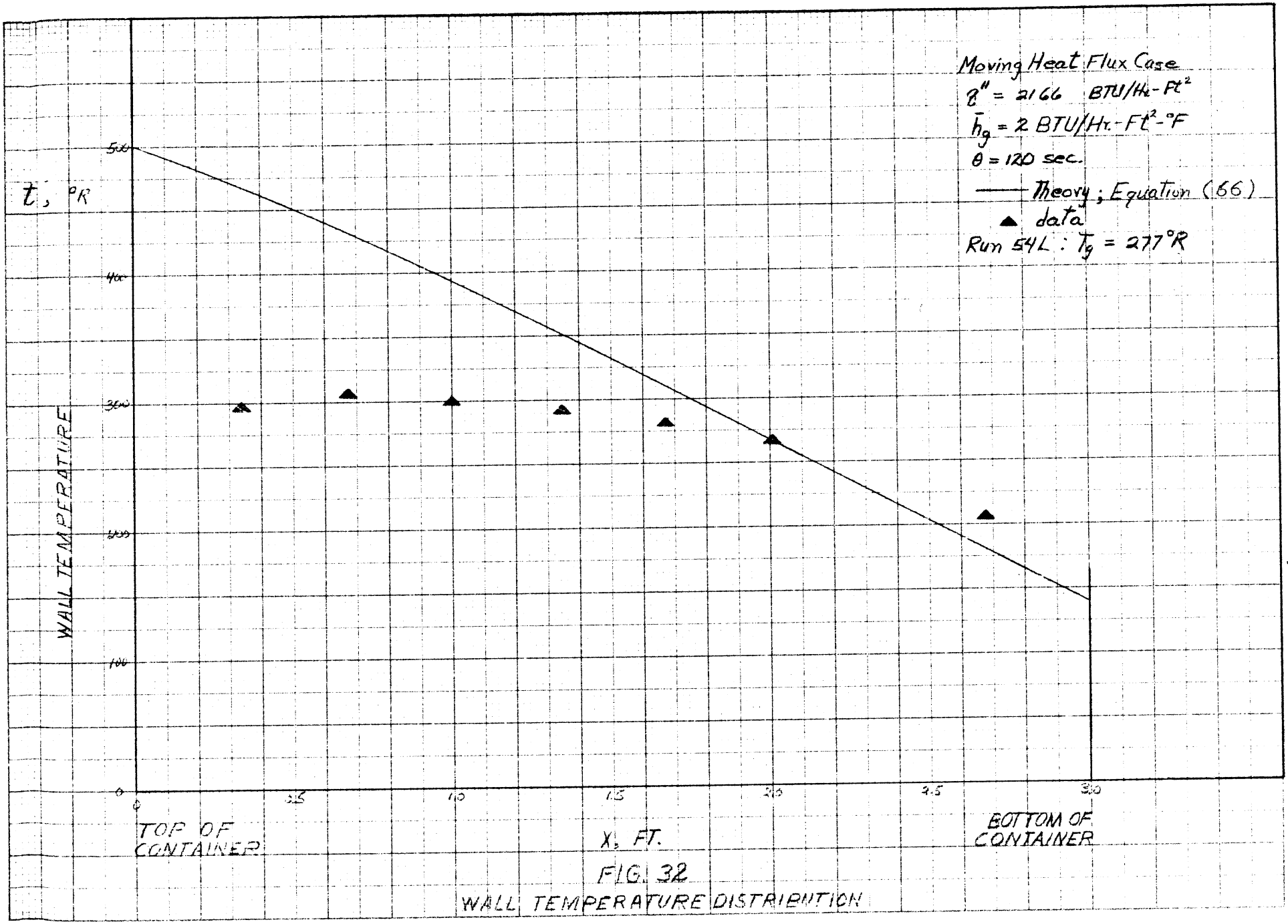

FIG. 32
WALL TEMPERATURE DISTRIBUTION

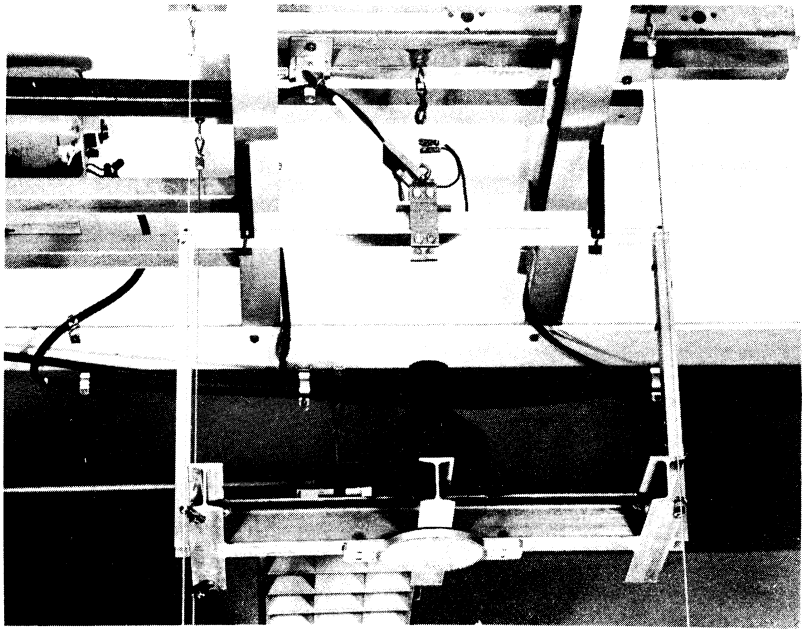

Fig. 34. Reduced gravity test assembly.

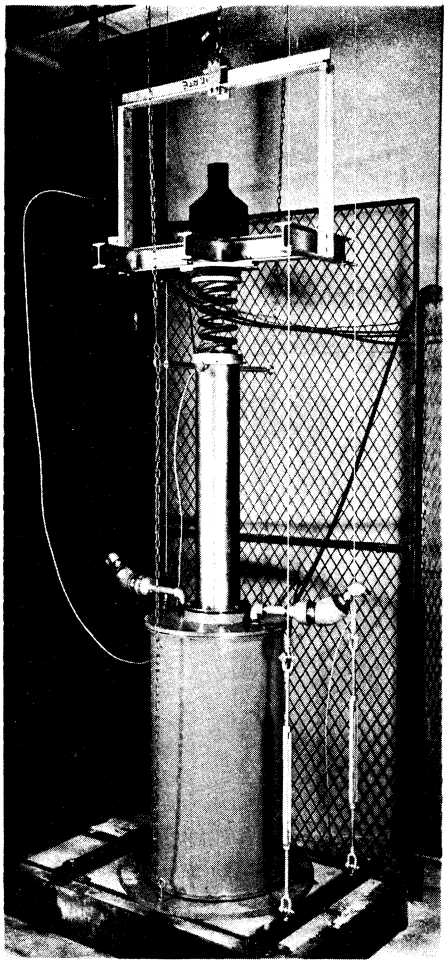

Fig. 35. Hydraulic buffer for arresting test assembly.

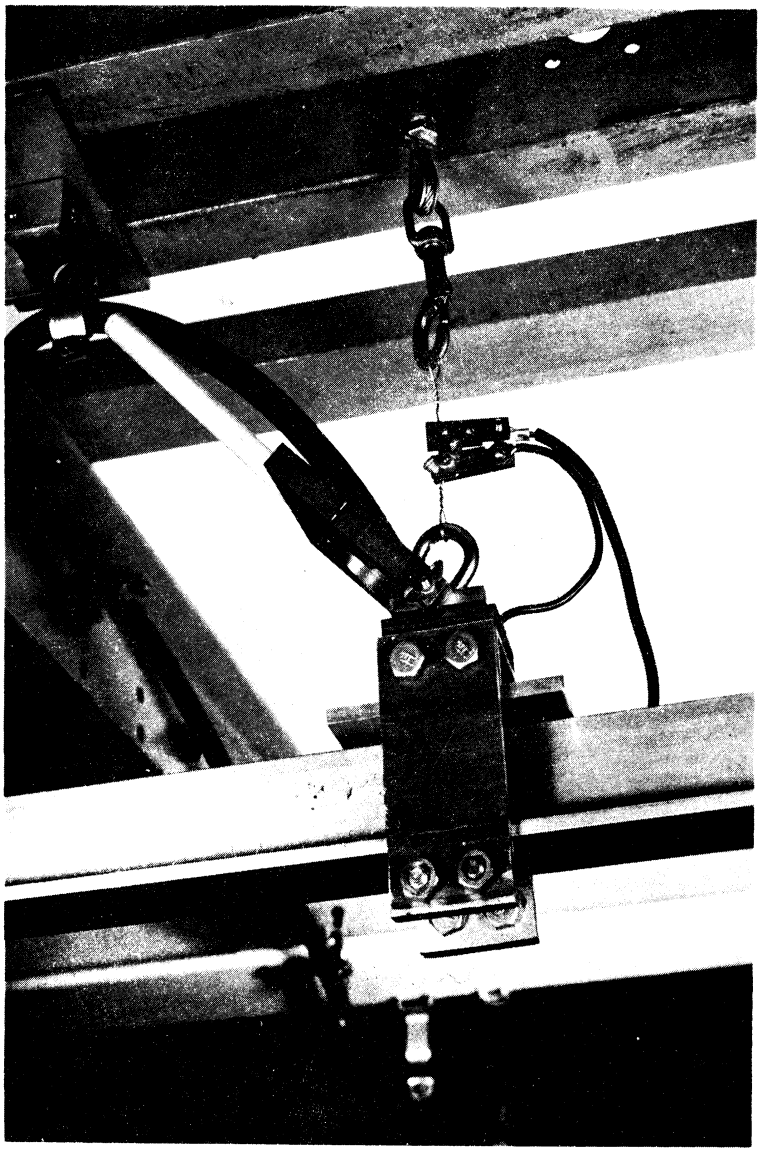

Fig. 36. Electrical release mechanism for test assembly.

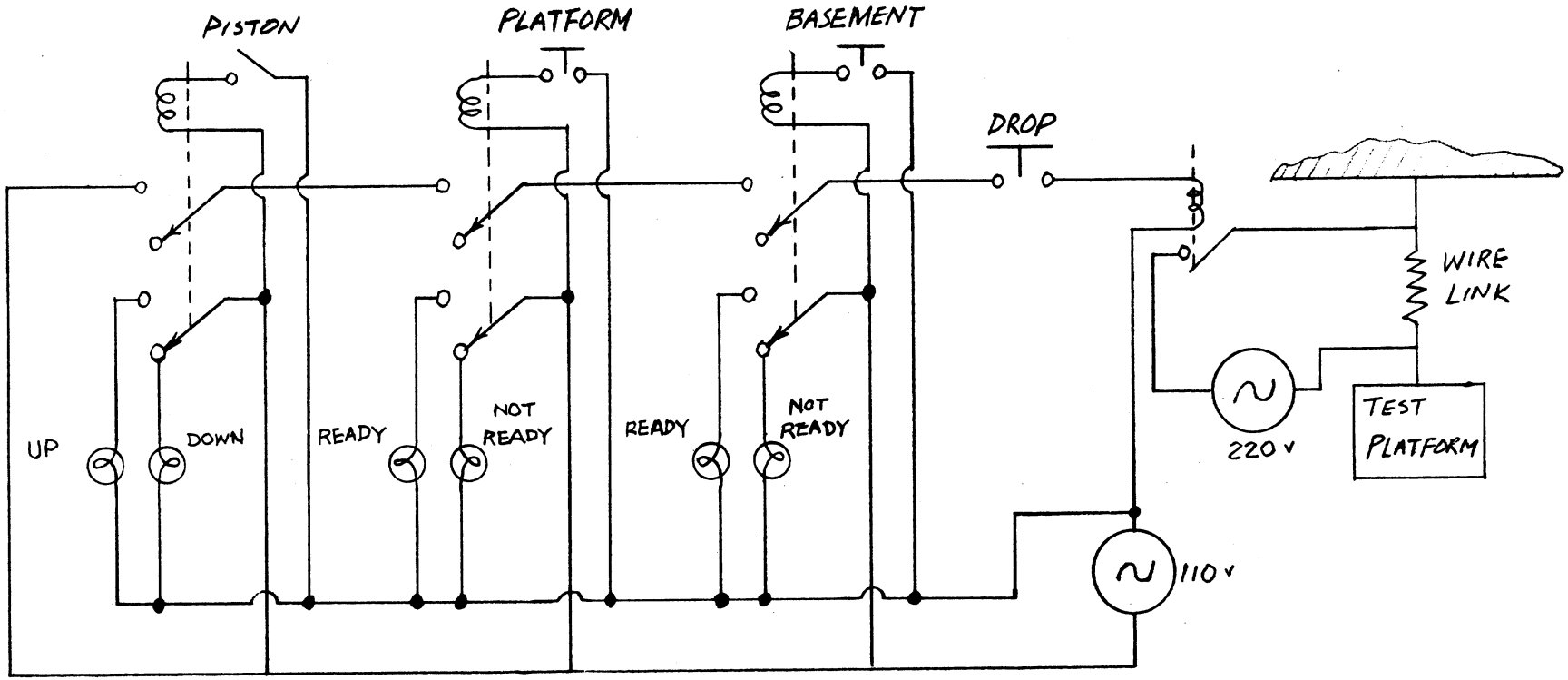

Fig. 37. Diagram of safety interlock system.

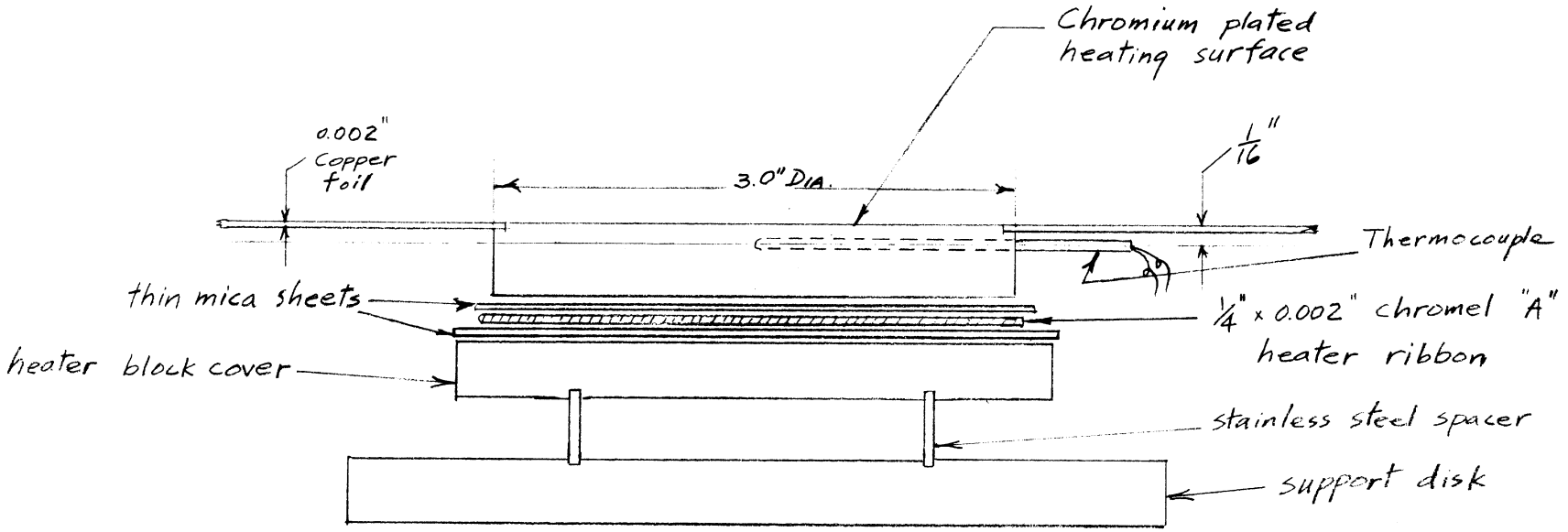

Fig. 38. Plate heating element for cryogenic fluids.

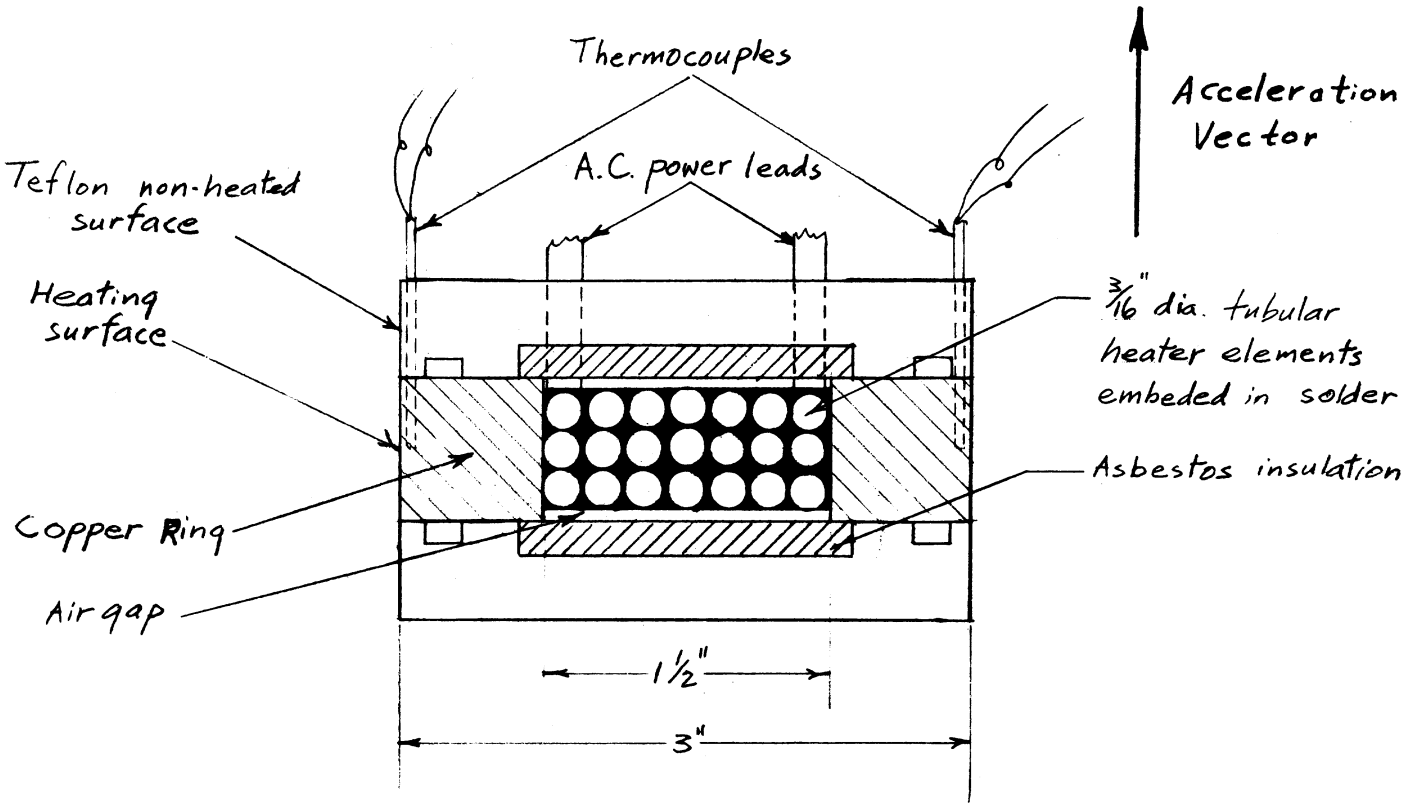

Fig. 39. Sketch of proposed vertically oriented surface for cryogenic fluids.